



**HAL**  
open science

## Geochemistry of the Society and Pitcairn-Gambier mantle plumes: what they share and do not share

Carole Cordier, H el ene Delavault, Catherine Chauvel

### ► To cite this version:

Carole Cordier, H el ene Delavault, Catherine Chauvel. Geochemistry of the Society and Pitcairn-Gambier mantle plumes: what they share and do not share. *Geochimica et Cosmochimica Acta*, 2021, 10.1016/j.gca.2021.04.014 . insu-03201535

**HAL Id: insu-03201535**

**<https://insu.hal.science/insu-03201535>**

Submitted on 19 Apr 2021

**HAL** is a multi-disciplinary open access archive for the deposit and dissemination of scientific research documents, whether they are published or not. The documents may come from teaching and research institutions in France or abroad, or from public or private research centers.

L'archive ouverte pluridisciplinaire **HAL**, est destin ee au d ep ot et  a la diffusion de documents scientifiques de niveau recherche, publi es ou non,  emanant des  tablissements d'enseignement et de recherche fran ais ou  trangers, des laboratoires publics ou priv es.

## Journal Pre-proofs

Geochemistry of the Society and Pitcairn-Gambier mantle plumes: what they share and do not share

Carole Cordier, H el ene Delavault, Catherine Chauvel

PII: S0016-7037(21)00229-5  
DOI: <https://doi.org/10.1016/j.gca.2021.04.014>  
Reference: GCA 12160

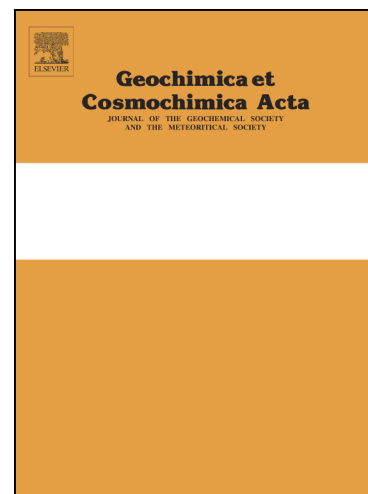
To appear in: *Geochimica et Cosmochimica Acta*

Received Date: 18 April 2020  
Revised Date: 23 March 2021  
Accepted Date: 7 April 2021

Please cite this article as: Cordier, C., Delavault, H., Chauvel, C., Geochemistry of the Society and Pitcairn-Gambier mantle plumes: what they share and do not share, *Geochimica et Cosmochimica Acta* (2021), doi: <https://doi.org/10.1016/j.gca.2021.04.014>

This is a PDF file of an article that has undergone enhancements after acceptance, such as the addition of a cover page and metadata, and formatting for readability, but it is not yet the definitive version of record. This version will undergo additional copyediting, typesetting and review before it is published in its final form, but we are providing this version to give early visibility of the article. Please note that, during the production process, errors may be discovered which could affect the content, and all legal disclaimers that apply to the journal pertain.

  2021 Elsevier Ltd. All rights reserved.



**Geochemistry of the Society and Pitcairn-Gambier mantle plumes: what they  
share and do not share**

Carole Cordier <sup>a,\*</sup>, H el ene Delavault <sup>a,1</sup>, Catherine Chauvel <sup>a,b</sup>

<sup>a</sup> Univ. Grenoble Alpes, CNRS, IRD, IFSTTAR, ISTerre, 38000 Grenoble, France

<sup>b</sup> Universit e de Paris, Institut de Physique du Globe de Paris, CNRS, F-75005 Paris, France

\* Corresponding author: [carole.cordier@univ-grenoble-alpes.fr](mailto:carole.cordier@univ-grenoble-alpes.fr)

<sup>1</sup> Current address: Thermo Fisher Scientific, 16 avenue du Qu ebec, BP 30210, 91941  
Villebon Courtaboeuf Cedex

**Abstract**

The South Pacific Superswell in Polynesia is associated with a large seismic mantle anomaly at depth, the Polynesian dome, and it is characterized by the volcanic activity of five different hotspots giving birth to the Marquesas, Society, Pitcairn-Gambier, Cook-Austral and Arago island chains. Here we present new isotopic and major and trace element data in basalts from two of these chains, the Society and Pitcairn-Gambier chains, in order to examine the similarities and differences of their mantle source regions. In the Society chain the entire geochemical diversity of the archipelago exists at the scale of individual islands with no systematic trend over time. In contrast, a clear geochemical dichotomy exists along the Pitcairn-Gambier chain between the old volcanoes (*Muru* basalts from Mururoa, Fangataufa, Gambier, > 5 My) and their younger counterparts (*Pitis* basalts from Pitcairn Island and Seamounts, <1 My). The *Muru* group has high  $Nb_N/Nb^*$  and Ce/Pb, low  $^{87}Sr/^{86}Sr$  and define a steep trend in Nd-Hf isotopic space, features that call for old eclogite in their mantle source. The unradiogenic Pb isotopic ratios of *Muru* basalts, well below the values observed in HIMU (“high  $\mu$ ”, or high  $^{238}U/^{204}Pb$ ) localities, are not easily explained by varying the age and composition of the eclogite and may call for the involvement of Pacific lower mantle in the source region. In contrast, the *Pitis* basalts share with the Society basalts low  $Nb_N/Nb^*$  and radiogenic  $^{87}Sr/^{86}Sr$  suggesting incorporation of continental material in their source region. While the Society source simply incorporates modern-like terrigenous sediments, the combination of low Ba/La,  $^{143}Nd/^{144}Nd$  and  $^{176}Hf/^{177}Hf$  and very high  $^{208}Pb^*/^{206}Pb^*$  in *Pitis* basalts make the *Pitis* source unique and not sampled anywhere else on Earth. The *Pitis* source contains old, possibly Archean, material of unclear origin because it resembles neither modern lower continental crust nor modern pelagic sediments. Finally, the distribution of heterogeneities in the two mantle plumes is also very different: discrete filaments are randomly dispersed across the Society plume stem while eclogitic and continent-derived

filaments are vertically separated under the Pitcairn-Gambier chain. By combining these results with those published for other Polynesian chains, we establish a snapshot of the composition, geometry and distribution of the crustal components present in the Polynesian dome.

Keyword: Mantle plume; French Polynesia; ocean island; canonical ratios; enriched mantle; EM1; EM2; plume structure

## I. Introduction

The geochemical characteristics of plume sources have been intensively investigated over the last decades. While radiogenic isotopes are used to characterize the diversity of mantle components in the source of ocean island basalts (OIB; e.g., White, 1985; Zindler and Hart, 1986; Hart, 1988; Hart et al., 1992; Hofmann, 1997), the trace-element variations are usually controlled by the extent of melting and/or the residual mineralogy in the plume source. However, some ratios of incompatible trace elements, the so-called canonical ratios (Ce/Pb and Nb/U as demonstrated by Hofmann et al., 1986), can prove useful to trace sources because (a) they are essentially unchanged during melting and fractional crystallization and (b) their values in the Earth mantle and continental crust are very different allowing quantification of potential mixing processes. Several authors have shown that changes of these canonical ratios were, in some cases, correlated to radiogenic isotopes (Weaver, 1991; Chauvel et al., 1992; White and Duncan, 1996; Woodhead, 1996; Willbold and Stracke, 2010; Hofmann, 2014), providing constraints on the origin of the isotopic diversity present in the Earth mantle.

Here, we evaluate the variations of isotopes and incompatible-trace element ratios in lavas from two Polynesian volcanic chains, the Pitcairn-Gambier and Society island chains, using a large geochemical dataset (major and trace elements and Sr-Nd-Hf-Pb isotope ratios). These two hotspots are located on a regionally shallow seafloor that stretches to two other active Polynesian hotspots (Marquesas and Cook-Austral; Fig. 1a, inset) and that is referred as the South Pacific Superswell. This superswell is linked to a seismic low-velocity anomaly located at the bottom of the Pacific upper mantle (McNutt and Judge, 1990; Adam and Bonneville, 2005) that could be due to the presence of a large dome at the transition zone

(Davaille, 1999; Kogiso, 2013; Obayashi et al., 2016) or the presence of plume cluster (Schubert et al., 2004). In the dome model, the different Polynesian plumes are secondary plumes coming from the dome (Courtillot et al., 2003) but given the isotopic diversity of Polynesian island chains, the composition of the material present in the dome must be very diverse (Kogiso, 2013; Chauvel et al., 2014).

The Pitcairn-Gambier and the Society chains plot along different trends in isotopic spaces, suggesting the presence of enriched material with different origin and composition in the source region of each hotspot. In addition, a large isotopic range exists along both chains suggesting temporal variability of the source composition. The Society basalts cover a large range of compositions that extend to low Ce/Pb and Nb/U and high  $^{87}\text{Sr}/^{86}\text{Sr}$  ratios compared to most OIB, a characteristic feature of Enriched Mantle-2 (EM2) mantle source domain usually attributed to the contribution of terrigenous sediments to the source (White and Hofmann, 1982; White, 1985; Hofmann et al., 1986; Zindler and Hart, 1986; Weaver, 1991; Chauvel et al., 1992; White and Duncan, 1996; Hémond et al., 1994). In addition, the entire geochemical diversity of the Society archipelago exists at the scale of individual islands and no age progression is observed (Cordier et al., 2015). By contrast, a clear temporal change of geochemical compositions exists along the Pitcairn-Gambier chain where the oldest islands (Mururoa, Fangataufa, Gambier) differ from their younger counterparts (Pitcairn Island and Seamounts). The oldest islands have positive Nb anomalies (high Nb/U) coupled with strong negative Pb (high Ce/Pb) anomalies but they do not have the radiogenic lead isotopes of typical High  $\mu$  basalts (HIMU; Vidal et al., 1984; Weaver, 1991; Zindler and Hart, 1986; Hart, 1988; Chauvel et al., 1992; Hauri and Hart, 1993). The current models for the mantle source of such lavas invoke the involvement of young oceanic crust (Vidal, 1992; Delavault et al., 2015) or that of lithospheric mantle metasomatized by HIMU-melts (Dupuy et al., 1993). In contrast to the oldest Pitcairn-Gambier islands, basalts from Pitcairn Island and

Seamounts have low Nb/U and Ce/Pb ratios, low  $^{206}\text{Pb}/^{204}\text{Pb}$  but high  $^{208}\text{Pb}/^{204}\text{Pb}$ , and low  $^{143}\text{Nd}/^{144}\text{Nd}$  (e.g., Woodhead and McCulloch, 1989; Eisele et al., 2002). For this reason, Pitcairn basalts are traditionally considered as the most extreme Enriched Mantle-1 (EM1) oceanic basalts (Zindler and Hart, 1986; Willbold and Stracke, 2010). The Pitcairn low Nb/U and Ce/Pb ratios are usually attributed to the presence of continental material in their mantle source region, but no consensus exists as for its type. Involvement of pelagic sediments with high Th/U – combined to a terrigenous fraction in some models – could explain the high  $^{208}\text{Pb}/^{204}\text{Pb}$  of Pitcairn basalts (Woodhead and McCulloch, 1989; Weaver, 1991; Chauvel et al., 1992; Woodhead and Devey, 1993; Dostal et al., 1998; Eisele et al., 2002; Garapić et al., 2015). Presence of lower continental crust or subcontinental lithospheric mantle in the source region of EM1 lavas has also been invoked, to explain the positive Eu anomalies of Tristan de Cunha basalts (Willbold and Stracke, 2010) and the Ce isotope compositions of Gough Island lavas (Boyet et al., 2019), respectively. By contrast, the discovery in Pitcairn lavas of sulfides with mass independent fractionation led Delavault et al. (2016) to propose that the recycled crustal material was at least 2.4 Ga-old and that it was more depleted in incompatible trace elements than clays or lower continental crust. Archean cherts (Delavault et al., 2016) and marine carbonates (Wang et al., 2018) could be suitable candidates to account for both the high  $^{208}\text{Pb}/^{204}\text{Pb}$  and low  $\delta^{26}\text{Mg}$  of Pitcairn lavas.

In this manuscript, we examine the similarities and differences in trace-element and isotope ratios between lavas from Pitcairn-Gambier and Society chains with the aim of providing new constraints to the potential origin of the enriched domains present in the mantle source region of both plumes. We then examine temporal changes along the Pitcairn-Gambier chain and how they could relate to the geometry of the heterogeneities within the plume stem. Finally, we compare this geometry with those of the Society, Marquesas, Cook-

Austral and Arago plumes to constrain the way small-scale heterogeneities occur in the Polynesian dome.

## 2. Geological setting

The Pitcairn-Gambier and Society chains are two of the five active Polynesian hotspots, together with Marquesas, Cook-Austral and Arago chains (Fig. 1a, inset). Both Society and Pitcairn-Gambier chains are oriented SE–NW, in the direction of the Pacific plate motion, and they are more than 1000 km apart from each other.

The Pitcairn-Gambier chain extends over more than 1000 km (Fig. 1a) and it has been active for at least 12 My. The oldest known volcanic activity was reported for Mururoa lavas that are now submerged under the atoll (11.9-10.7 My; Gillot et al., 1992). It was followed by Fangataufa volcano (11.8 to 10.0 My; Guillou et al., 1990), Gambier archipelago (7.1 to 5.8 My; Caroff et al., 1993), Pitcairn Island (0.95 to 0.62 My; Duncan et al., 1974), and the volcanically active Pitcairn Seamounts (Woodhead and Devey, 1993). The age progression along the entire chain corresponds to the Pacific plate velocity (Fig. 1a; Duncan and McDougall, 1976; Guillou et al., 1990), which suggests that the Pitcairn-Gambier chain was built by a single plume. Several seamounts exist between Gambier and Pitcairn Islands (Fig. 1a) but both their age and composition are unknown.

The 700-km long volcanic chain of the Society Islands (Fig. 1b) was built during the last 5 My. The chain includes 9 islands, together with atolls and seamounts. The island of Maupiti, dated at ~ 4.5 My (Blais et al., 2002), is the oldest subaerial expression of the hotspot; the youngest plume activity is observed at the south-eastern end of the chain, with the island of Mehetia (< 0.6 My; Blais et al., 2002) and a dozen adjacent seamounts (Devey et al., 2003).

### 3. Material and methods

#### 3.1 Material

Samples of Pitcairn-Gambier lavas come from the Viviane drill core at Mururoa (Caroff, 1992) and the Echo1 drill core at Fangataufa (Guillou, 1990); samples from Gambier and Pitcairn Islands were collected in the field during the course of two Ph.D. research projects (Binard, 1991; Caroff, 1992) while samples from Pitcairn Seamounts were dredged on Bounty and Adams submarine edifices during the SO-65 campaign of the German Research Vessel "SONNE" in 1989 (Stoffers et al., 1990). Samples from six islands of the Society chain (Fig. 1b) were recovered in the nineties by the Bureau de Recherches Géologiques et Minières (BRGM, France) and during two Ph.D. projects (Binard, 1991; Le Dez, 1996).

A partial geochemical dataset already exists on selected samples: concentrations of major and some trace elements were measured by inductively coupled plasma atomic emission spectroscopy (ICP-AES) and reported in notices of geological maps, French publications or Ph.D. theses (Achard; 1987; Guillou; 1990; Binard, 1991; Caroff; 1992; Caroff et al., 1993; Binard et al., 1993; Le Dez, 1996; Blais et al., 2000, 2002, 2004, 2006; Maury et al., 2001; Legendre et al., 2003). These data are combined with Sr-Nd-Hf-Pb isotope ratios for 16 samples from Pitcairn Island and Seamounts (Delavault et al., 2016) and 68 samples from the Society chain (Cordier et al., 2016). In addition, 25 lavas from Gambier Island analyzed by Delavault et al. (2015) are included in the dataset because they used the same analytical procedures. Our new analyses are for (1) major-element concentrations of 10 samples from Pitcairn-Gambier, (2) trace-element contents of 124 samples of both chains

determined by inductively coupled plasma mass spectrometry (ICP-MS), and (3) isotope ratios of 18 samples from Pitcairn-Gambier. Altogether, this provides a consistent set of 145 samples with complete geochemical data all determined on the same samples and using the same procedures.

### 3.2 Major and trace elements

All samples were crushed in an agate mortar. Major elements were measured by ICP-AES in Grenoble, using the method described by Chauvel et al. (2011). The signal was calibrated using BHVO-2. Typical accuracy and reproducibility were established by repeated measurements of the geological reference materials BCR-2, BR24 and BEN, and are better than 2.5 % ( $2\sigma$ ) for  $\text{SiO}_2$ , and better than 5 % for other elements. Trace elements were measured using ICP-MS technique on the Agilent 7500ce instrument in Grenoble and following the method described in Chauvel et al. (2011). For most elements, both precision and reproducibility were better than 5 %, as confirmed by the analyses of the geological reference materials BEN, BHVO-2 and AGV-1 run as unknown (Table S1a) and duplicate analyses of several samples (Table S1b).

### 3.3 Sr-Nd-Hf-Pb isotopes

Nd, Hf, Pb, and Sr were isolated using ion-exchange chromatography techniques described in Chauvel et al. (2011). The blanks were on average 84 pg for Nd ( $n = 8$ ), 28 pg for Hf ( $n = 5$ ), 76 pg for Pb ( $n = 6$ ), and 23 pg for Sr ( $n = 2$ ). Duplicate analyses are given in Table S1c. Nd, Hf, and Pb isotopic compositions were measured on a high-resolution multicollector ICP-MS (Nu Instrument 1700) at ENS Lyon. The Hf and Nd isotopic data were

corrected for mass fractionation bias using  $^{179}\text{Hf}/^{177}\text{Hf} = 0.7325$  and  $^{146}\text{Nd}/^{144}\text{Nd} = 0.7219$ . The average  $^{143}\text{Nd}/^{144}\text{Nd}$  of the Nd Ames-Rennes standard was  $0.511967 \pm 30$  ( $2\sigma$ ,  $n = 43$ ) and the average  $^{176}\text{Hf}/^{177}\text{Hf}$  of the Hf Ames-Grenoble standard was  $0.282156 \pm 12$  ( $n = 26$ ). Both standards were run every 2 or 3 samples, and any potential drift was corrected using the recommended values of  $^{143}\text{Nd}/^{144}\text{Nd} = 0.511960$  (Chauvel and Blichert-Toft; 2001) and  $^{176}\text{Hf}/^{177}\text{Hf} = 0.282160$  (Chauvel et al.; 2011). For Pb, mass fractionation bias was corrected using a Tl tracer (White et al., 2000) and instrumental drift was corrected using the standard bracketing method: the NBS981 standard was run every 2 or 3 samples and Pb isotope ratios were corrected to the values recommended by Jochum et al. (2011) ( $^{208}\text{Pb}/^{204}\text{Pb} = 36.7309$ ,  $^{207}\text{Pb}/^{204}\text{Pb} = 15.5011$ ,  $^{206}\text{Pb}/^{204}\text{Pb} = 16.9435$ ). Sr isotopic compositions were measured on a Thermo Scientific Triton TIMS at PSO-IUEM (Brest) during 2 different sessions. Because the average values obtained for the NBS987 standard differ slightly between the two sessions ( $0.710241 \pm 14$ ,  $n = 7$ ; and  $0.710231 \pm 10$ ,  $n = 16$ ), we normalized all measured  $^{87}\text{Sr}/^{86}\text{Sr}$  to the recommended standard value of 0.710250 (McArthur, 1994).

## 4. Results

### 4.1 A basalt dataset

The new coherent set of data for Pitcairn-Gambier and Society chains is given in Table S2. New data cover a wide range of composition, from picritic basalts to trachyphonolites, with  $\text{SiO}_2$  ranging from 40 to 67 wt% and MgO from 0 to 24 wt% (Figs 2 and S3). High-MgO lavas ( $> 15$  wt%) are sampled at Gambier, Huahine, Raiatea, Moorea, and Mehetia islands (Fig. 2). Evolved lavas with low MgO contents ( $< 4.5$  wt%) are abundant at Raiatea and Pitcairn Island and Seamounts (Fig. 2).

In order to minimize the effect of differentiation on incompatible trace-element ratios, we use a subset of these data to focus on the mafic compositions from each locality. Mafic lavas being rare at Pitcairn Island and Seamounts (Fig. 2), we looked for a good compromise between number of samples and limited effect of differentiation, considering that olivine fractionation does not noticeably change most incompatible trace-element ratios.

Fractionation and accumulation of other mineral phases were evaluated from variations of  $\text{CaO}/\text{Al}_2\text{O}_3$  with MgO (Fig. 2). At each island,  $\text{CaO}/\text{Al}_2\text{O}_3$  is more or less constant in samples with MgO values higher than 4.5 wt%. At lower MgO,  $\text{CaO}/\text{Al}_2\text{O}_3$  drastically decreases, as well as CaO and  $\text{TiO}_2$  contents (Fig. S3), highlighting the onset of clinopyroxene  $\pm$  amphibole  $\pm$  plagioclase  $\pm$  Fe-Ti oxide fractionation. We thus do not further discuss the differentiated lavas (MgO < 4.5 wt%). Most of the high-MgO rocks (MgO > 15 wt%) have constant  $\text{CaO}/\text{Al}_2\text{O}_3$  (Fig. 2). They plot on the olivine control lines in the variation diagrams of Figure S3 and they have high Ni contents (> 450 ppm, Table S1), suggesting they formed by accumulation of olivine. Still, some samples show textural and geochemical evidence for clinopyroxene and olivine accumulation, which leads us to exclude all lavas with MgO > 15 wt% from our selection. Finally, we disregarded weathered samples identified by loss on ignition (LOI) value higher than 3 wt% or elevated ratios of fluid-mobile elements, such as Ba/Th (e.g., Ba/Th = 195 in HA-123 while the average for the dataset is  $80 \pm 13$ ). The screened dataset consists in 122 samples (Table S1) and for simplicity, we will refer to all these lavas as basalts, even if this nomenclature is not strictly correct.

In figures and tables we also report a compilation of literature data for basalts from Pitcairn-Gambier and Society chains and from seven other OIB chains characteristic of mantle components (HIMU: St Helena and Mangaia, Tubuai and the old lavas of Rurutu island in the Cook-Austral chain; HIMU-like: Canary Islands, EM2: Samoan and Marquesas Islands; EM1: Tristan da Cunha and Walvis Ridge). This compilation is built using the

GEOROC database, accessed in July 2019. We exclude all samples from post-shield and rejuvenated stages, having high LOI or H<sub>2</sub>O contents (>3 wt %), or MgO contents lying outside the 4.5 - 15 wt% range. Finally, we only include in the compilation samples for which two isotope ratios are given and for which we can calculate Ce/Pb or  $Nb_N/Nb^* = Nb_N/(Th_N \times La_N)^{1/2}$ , the subscript <sub>N</sub> indicates concentrations normalized to the primitive-mantle values of McDonough and Sun (1995). At the end of the selection procedure, the literature compilation includes 50 samples from the Pitcairn-Gambier chain, most of them from Pitcairn Island and Seamounts (36 samples), together with 20 samples from the studied volcanoes of the Society chain. References for these literature data are given in the figure caption of Figure S3.

#### 4.2 Major element variations in the basalt dataset

Basaltic lavas from Pitcairn-Gambier and Society chains vary from tholeiitic to alkali basalts (Fig. S3a). The basalts from Mururoa are alkali, while all Gambier basalts are tholeiitic, and Fangataufa basalts are either alkali or tholeiitic. Basalts from Pitcairn Island and Seamounts investigated here are all alkali, but tholeiitic compositions have been reported for Pitcairn Seamounts by Woodhead and Devey (1993), Eisele et al. (2002) and Hékinian et al. (2003). All basalts from the Society chain considered in our study are alkali.

The basalts have roughly constant CaO/Al<sub>2</sub>O<sub>3</sub> ratio (~ 0.8, Fig. 2), as a result of our selection method, but variations are observed from island to island. These variations are coupled with difference in TiO<sub>2</sub> content at a given MgO (Fig. S3d) and might, therefore, trace difference in source lithology (peridotite versus eclogite and pyroxenite; Kogiso and Hirschmann, 2006). Amongst Pitcairn-Gambier lavas, basalts from Pitcairn Island and Seamounts have distinctly low CaO/Al<sub>2</sub>O<sub>3</sub> ( $0.60 \pm 0.06$ , Table 1 and Fig. 2) while lavas from Mururoa have high CaO/Al<sub>2</sub>O<sub>3</sub> ( $0.82 \pm 0.04$ ) coupled with high TiO<sub>2</sub> ( $\geq 4$  wt%, Fig. S3d).

Along the Society chain, the highest CaO/Al<sub>2</sub>O<sub>3</sub> ratios (> 0.8, Fig. 2) and TiO<sub>2</sub> contents (~ 3 wt%, Fig. S3d) are observed for Raiatea and Mehetia basalts, while the lowest values correspond to basalts from Huahine and Maupiti.

#### 4.3 Incompatible trace-element patterns of basalts

Incompatible trace-element patterns in representative basalts are shown in Figure 3. The patterns of all samples are shown in Figure S4 for Pitcairn-Gambier chain and in Figure S5 for Society chain. The basalts are all enriched in the most incompatible elements, with (La/Sm)<sub>N</sub> ratios ranging from 1.5 to 4 (Table 1). Basalts of Gambier Island tend to have low (La/Sm)<sub>N</sub> (1.7 to 2.4, Table 1) compared to other islands, a feature consistent with the tholeiitic composition of these samples suggesting they form by higher degrees of melting. All studied basalts have fractionated Heavy Rare Earth Elements (HREE), with (Dy/Yb)<sub>N</sub> ratios of  $1.8 \pm 0.2$  in Pitcairn-Gambier basalts and  $2.1 \pm 0.2$  in Society basalts (Table 1), suggesting that melting of plume material occurred in the garnet stability field.

Two groups of basalts can be distinguished along the Pitcairn-Gambier chain due to differences in Nb-Ta enrichment and, to a lesser extent, Pb depletion relative to neighbor elements in Figure 3a. Basalts from Mururoa, Fangataufa and Gambier show systematic positive anomalies in Nb-Ta and, commonly, strong negative anomalies in Pb. Basalts from Pitcairn Island and Seamounts, on the other hand, lack the positive Nb-Ta anomaly and show negative Pb anomalies of lower magnitude. Along the Society chain (Figs 3b and S5), the trace-element patterns of basalts resemble those of Pitcairn Island and Seamounts with no positive Nb-Ta anomaly and, commonly, slight to moderate negative Pb anomalies. Three lavas from Mehetia show positive Pb anomalies (Fig. S5).

#### 4.4 Radiogenic isotopes

Sr-Nd-Hf ratios are shown in Figure 4 and variation ranges of Sr-Nd-Hf-Pb ratios in each volcano are listed in Table 1. Our new data are for Mururoa, Fangataufa and a few samples from Gambier Island. Age correction was not applied on these new analyses because all have low parent/daughter ratios ( $Rb/Sr < 0.04$ ;  $Lu/Hf < 0.06$ ;  $Sm/Nd < 0.25$ ;  $U/Pb < 0.44$ ;  $Th/Pb < 1.76$ ; Table S2) and radiogenic growth since lava emplacement is smaller than the analytical errors. To our knowledge, the Hf isotopic analyses for Mururoa and Fangataufa basalts are the first reported in literature.

Isotopic compositions of new samples from Gambier Island are consistent with data published by Delavault et al. (2015) and integrated to our dataset (Fig. 4). As for incompatible trace elements, Mururoa and Fangataufa basalts show isotope ratios similar to Gambier samples, with low  $^{87}Sr/^{86}Sr$  and relatively elevated  $^{143}Nd/^{144}Nd$  and  $^{176}Hf/^{177}Hf$ , though some consistent differences between volcanoes are noticeable. Mururoa lavas have slightly higher  $^{87}Sr/^{86}Sr$  than the two other islands, as already pointed out by Dupuy et al. (1993), and  $^{143}Nd/^{144}Nd$  and  $^{176}Hf/^{177}Hf$  increase from Mururoa to Fangataufa to Gambier. Sr-Nd-Hf isotopic compositions, and notably the steep trend in Nd-Hf isotopic space (Fig. 4b), resemble those reported for HIMU basalts, such as St Helena and Tubuai, Mangaia and Rurutu (older volcanic serie) in the Cook-Austral chain. However, Pb isotope ratios at Mururoa, Fangataufa and Gambier are low (e.g.  $^{206}Pb/^{204}Pb < 19.6$ , Figs 4c and d) compared with values known in HIMU basalts ( $^{206}Pb/^{204}Pb > 19.6$ , Figs 4c and d).

Our new isotopic data on Mururoa and Fangataufa basalts confirm the clear isotopic distinction between the older basalts from Mururoa, Fangataufa and Gambier; and the younger lavas from Pitcairn Islands and Seamounts. Not only the isotopic ranges do not overlap but the two groups of lavas also form arrays with distinct slopes in Figure 4. This

means that each group of islands derives from regions of the plume having different isotopic compositions.

## 5. Discussion

### 5.1 Tracing source composition: incompatible trace elements and isotopes

#### 5.1.1 Nb and Pb anomalies, a source feature

We quantify the Nb-Ta and Pb anomalies in incompatible trace-element patterns using the  $Nb_N/Nb^*$  and Ce/Pb ratios, as listed in Table 1. We prefer the  $Nb_N/Nb^*$  ratio to the canonical Nb/U ratio, because it is less dependent on U concentration and is considered as a robust proxy for the Nb anomaly (Weaver, 1991; Eisele et al., 2002; Hofmann, 2014).

The most striking observation is that two groups of basalts can be distinguished due to differences in  $Nb_N/Nb^*$  ratios, as shown in Figure 5. Basalts with high  $Nb_N/Nb^*$  ratios ( $>1.4$ ) mostly come from Mururoa, Fangataufa and Gambier, i.e. the oldest volcanoes of the Pitcairn-Gambier chain (age  $> 5$  My, Fig. 1). These basalts are hereafter referred to as the *Muru* group, in reference to Mururoa, the oldest volcano. *Muru* lavas also tend to have pronounced negative Pb anomalies, resulting in Ce/Pb ratios mostly higher than 22 (Fig. 5a).

The group with low  $Nb_N/Nb^*$  ratios (mostly  $< 1.4$ , Fig. 5) includes most young ( $< 1$  My) basalts from Pitcairn Island and Seamounts, hereafter called the *Pitis* group, an acronym for Pitcairn Island and Seamounts, as well as basalts from the Society chain. In the Pitcairn-Gambier chain, *Pitis* basalts also differ from *Muru* lavas by their low Ce/Pb (mostly  $< 24$ , Fig. 5a and Table 1). While having similarly low  $Nb_N/Nb^*$  ratios, basalts from the Society chain show a wider range of Ce/Pb ratios than the *Pitis* basalts (8 to 32, Fig. 5a and Table 1). In

general terms, basalts from the *Pitis* group and Society chain are quite similar in terms of trace-element systematics, but Society basalts are less depleted in Ba resulting in higher Ba/La and Ba/Th ratios (e.g., Ba/La = 7 to 19 in Society chain versus < 9 for the *Pitis* group, Fig. 5b and Table 1).

Variations of  $Nb_N/Nb^*$ , Ce/Pb and Ba/La ratios between *Muru*, *Pitis* and Society lavas could result from crystallization and partial melting processes. We show in Figure S6 that none of these ratios correlates with MgO content, which suggests that their variations are not controlled by crystallization. Determining the impact of partial melting is more complex. In Figures 5c and d, we show how  $Nb_N/Nb^*$ , Ce/Pb and Ba/La ratios vary in melts as a function of melting rate, source composition and lithology. The various curves are calculated using a non-modal batch melting equation and five different source compositions: the depleted mantle of Salters and Stracke (2004) [DMM]; an eclogite with a dehydrated MORB composition (Kogiso et al., 1997; Gale et al., 2013) [OC]; terrigenous sediments (GLOSS-II; Plank, 2014) [Terr. seds]; pelagic sediments (Plank and Langmuir, 1998) [Pel.seds]; and the average lower continental crust of Rudnick and Gao (2003) [LCC]. Mixtures of depleted mantle and the four recycled materials are also shown (see Figure 5d for details). All parameters are given in Table S7. The melting curves shown in Figures 5c and d show that  $Nb_N/Nb^*$  is independent of the melting degree for all sources other than recycled oceanic crust [OC], in which it increases slightly when melting of eclogite proceeds because Nb is less incompatible than La and Th in garnet according to Salters and Stracke (2004) and garnet preferentially enters the melt during partial melting of eclogite (Sobolev et al., 2000). However, the total range of  $Nb_N/Nb^*$  that could be attributed to melting remains very small compared with the range resulting from differences in source composition. As shown in Figures 5c and d, 10% of oceanic crust in the source generates melts with high  $Nb_N/Nb^*$  (> 1.6) compared with melts generated by melting only depleted mantle ( $Nb_N/Nb^* \sim 1.3$ , brown dashed line in Figs 5c and

d). In contrast, 10% of continental material is enough to reduce drastically the  $Nb_N/Nb^*$  to values lower than 0.6. We can therefore confidently assume that the  $Nb_N/Nb^*$  variations seen in our dataset (0.6 to 1.9; Figs 5a and b) trace differences in source compositions.

Melting processes have more impact on Ba/La and Ce/Pb ratios because Ce and La are significantly less incompatible than Pb and Ba in clinopyroxene when using Salters and Stracke (2004) partition coefficients (Table S7); significant ranges are therefore created when melt fractions vary between 1% and 10% (Figs 5c and d). However, large differences in Ba/La and Ce/Pb ratios can only be explained by differences in source composition: the involvement of continental material is required to obtain Ce/Pb values as low as 10 (Fig. 5c) and that of oceanic crust to have Ce/Pb ratios in melts higher than 30. Figure 5d shows how Ba/La varies depending on the composition of the source and the melting degree and it is helpful to discuss the nature of the continental material present in the source: the involvement of both lower continental crust and terrigenous sediments leads to high Ba/La melts while melts produced from pelagic sediments have low Ba/La. However, one should be cautious because the composition of pelagic sediments is highly variable, particularly for Ba content (300 to 2000 ppm; Plank and Langmuir, 1998; Porter and White, 2009). In summary, even if partial melting can blur the message carried by  $Nb_N/Nb^*$ , Ce/Pb and Ba/La, the observed differences between *Muru*, *Pitis* and *Society* groups require that sources are different and include recycled materials of diverse origins.

$Nb_N/Nb^*$ , Ce/Pb and Ba/La ratios in Pitcairn-Gambier and Society basalts vary with radiogenic isotopes (Fig. 6) demonstrating the ancient origin of the trace-element fractionations. In the  $Nb_N/Nb^*$  versus  $^{87}Sr/^{86}Sr$  diagram of Figures 6a, the high  $Nb_N/Nb^*$  *Muru* group also has distinctly low Sr isotopic compositions while the *Society* and *Pitis* groups both have more radiogenic Sr and cannot be distinguished. In contrast, when  $^{143}Nd/^{144}Nd$ ,  $^{176}Hf/^{177}Hf$  or  $^{208}Pb^*/^{206}Pb^*$  is plotted as a function of  $Nb_N/Nb^*$  (Figs 6b-d), a

clear distinction appears between the Society and *Pitis* groups. The *Pitis* group with its low  $^{143}\text{Nd}/^{144}\text{Nd}$  and its high  $^{208}\text{Pb}^*/^{206}\text{Pb}^*$  requires a source much older and/or much more enriched in LREE and Th relative to U. In the next section, we try to evaluate how accurately we can model the long-term isotopic evolution of radiogenic systems.

### 5.1.2 How reliable are radiogenic isotopes mixing arrays?

Figures 4a and b show that the three groups (*Muru*, *Pitis* and Society) define three separate trends in Hf, Nd and Sr isotopic spaces. Basalts from the Society chain and *Pitis* group have distinct isotopic compositions that extend toward EM2 composition (Society chain) and EM1 composition (*Pitis* group) and *Muru* group points to low Hf isotopes similar to what is observed in HIMU basalts. Each isotopic array can be interpreted as mixing array between depleted and enriched end-members. When looking at how isotope ratios relate to indicators of melting degree, such as  $\text{La}/\text{Sm}_\text{N}$  or alkalinity (Fig. S8), it appears that the mixing arrays are partly governed by melting processes, especially in the *Pitis* and *Muru* groups: low-degree melts have high  $\text{La}/\text{Sm}_\text{N}$  and  $(\text{Na}_2\text{O}+\text{K}_2\text{O})/\text{SiO}_2$  and they have the most enriched compositions of each group while high-degree melts tend to have more depleted compositions. This implies that mixing between depleted and enriched source components probably arises during progressive melting of the heterogeneous mantle column, in which the enriched components preferentially melt at low temperature (Phipps Morgan, 1999; Ito and Mahoney, 2005). Such process causes the relative proportion of melts from enriched and depleted material to vary in function of the melting degree and produces the isotopic mixing trends observed in our dataset. Modeling this melting-induced mixing is complicated because it requires assumptions on the melting behavior of the enriched material (e.g., Ito and Mahoney, 2005) so we simplified the case by considering that mixing occurs in the solid

state. This allows us to place constraints on the origin of the depleted and enriched materials in the mantle source region of *Muru*, *Pitis* and Society basalts, but their exact proportion in the source region is not quantified.

The trace element features described above suggest strongly that the enriched components result from the recycling in the mantle of continental and oceanic crustal materials. The present-day isotopic composition of any recycled material depends on its parent/daughter ratio, its isotopic ratio at the time of recycling into the mantle ( $T_R$ ) and the time interval since recycling. To model this evolution, we adopted the same approach as Stracke et al. (2003) and Delavault et al. (2015) and we modeled the isotopic composition of recycled oceanic crust and continental sediments. Details are given in Table S9. The pitfall of such calculation is that it implies good knowledge of the parent-daughter ratios of several crustal materials once they are recycled into the mantle. However, this is clearly not the case for a number of reasons: (1) present-day MORB and continental sediments cover a wide range of chemical compositions (e.g., Gale et al., 2013; Plank, 2014) with a poorly constrained average value; (2) subduction processes modify the parent-daughter ratios and again this is poorly constrained (Table S9). In Figure 7, we show how the isotopic compositions of recycled material vary depending on material composition, subduction fluxes and age. The modeled field for recycled oceanic crust defines a narrow band in Hf versus Nd isotopic space but a large field in Hf versus Pb isotopic space (Figs 7a and b). This is mainly due to the age of the recycled material, but changing the nature of the oceanic crust (depleted to enriched MORB) or the element mobility factor during dehydration in the subduction zone also has a significant impact. Similarly, we show modeled fields for pelagic and terrigenous sediments that have been partially melted or dehydrated during subduction, using the chemical budget of Johnson and Plank (1999) and Porter and White (2009). Panels a and b of Figure 7 show clearly that the age of the recycled sediment is an important parameter but they also show that

changing the element mobility during subduction introduces a large range of possible values at any time  $T_R$ . This is particularly true for recycled terrigenous sediments in Hf - Pb isotopic space (Fig. 7b). More surprisingly, the choice of isotopic compositions for the source of present-day MORB (DMM) has significant impact of the composition of the old recycled oceanic crust as shown by the difference between the orange (DMM after Stracke et al., 2003) and blue (DMM after Delavault et al., 2015) fields in panels c and d of Figure 7. Unfortunately, the impact of the choice of DMM cannot be distinguished from a difference in age of the recycled crust in these isotopic spaces. Given all these poorly known parameters, the age and the exact proportion of recycled material in the source of a given ocean island cannot be precisely determined using such modeling. We will therefore focus the rest of the discussion on the origin of the material recycled into the mantle source region of each basalt groups.

## 5.2 Origin of high $Nb_N/Nb^*$ *Muru* basalts

Basalts of the *Muru* group share lots of features with HIMU islands: they have high  $Nb_N/Nb^*$  and high Ce/Pb (Fig. 5c), and they define a steep trend in the Nd-Hf isotopic space, below the mantle array reference line (Fig. 4b). However, *Muru* basalts also have slightly higher  $^{87}Sr/^{86}Sr$  ratios than HIMU lavas and, more importantly, they lack the radiogenic Pb ratios that characterize HIMU islands ( $^{206}Pb/^{204}Pb < 19.5$  versus  $> 20.5$ , Figs 4c and d). In the  $^{207}Pb$ - $^{206}Pb$  isotopic space of Figure 4c, *Muru* basalts also have low  $^{207}Pb/^{204}Pb$  ratio at a given  $^{206}Pb/^{204}Pb$  compared to most other OIB, but they resemble HIMU-like lavas such as the basalts from Canary Islands.

For a long time, the high Ce/Pb and Nb/U ratios, as well as the radiogenic Pb and the steep Hf-Nd isotopic array of HIMU and HIMU-like basalts were best explained by the

involvement of old ( $> 2$  Gy) recycled oceanic crust, with minor or no contribution of continental sediments (Dupuy et al., 1989; Chauvel et al., 1992, 2008; Salters and White, 1998; Stracke et al., 2003, 2005; Béguelin et al., 2017). However, more recently, Herzberg et al. (2014) and Weiss et al. (2016) argued that the composition of olivines present in Mangaia and Tubuai HIMU basalts suggested an eclogite-free mantle source region based on the Sobolev et al. (2007) classification. Alternative scenarios for the origin of the HIMU source have thus been proposed and these include interaction of the mantle with partial melts derived from subducted oceanic crust (Hanyu et al., 2011; Herzberg et al., 2014) or with slab-derived carbonatitic or supercritical fluids (Weiss et al., 2016; Pettke et al., 2018). The olivine of Gambier basalts from the *Muru* group have been analyzed by Delavault et al. (2015); they are rich in Ni and poor in Fe and Mn, compositions that strongly support the presence of eclogite in the *Muru* source region. By combining olivine composition with incompatible trace-element contents and isotope ratios of the host lavas, Delavault et al. (2015) demonstrated that the source of Gambier basalts should contain  $\sim 5\%$  of a 1.5 Gy eclogite made of oceanic crust with up to 3% of continental sediments and we will discuss this interpretation for the whole *Muru* group.

Subtle chemical differences exist between lavas from the three locations of the *Muru* group and the clearest trend appears in Hf – Nd isotopic space (Figure 4b) with Mururoa being the most extreme followed by Fangataufa and Gambier. Such trend could be explained by the presence of an increasingly younger eclogite in the source region from Mururoa to Gambier (Fig. 7). However, the isotopic differences are coupled with variations of the extent of melting (Fig. S8), as shown by the low alkalinity and low  $(La/Sm)_N$  ratios of Gambier basalts compared to Mururoa lavas, Fangataufa samples having transitional compositions. As a consequence, even if we did not measure olivine compositions at Mururoa and Fangataufa, we can suggest that melts derived from the more fusible eclogite are progressively diluted in

melts derived from the ambient peridotite when the melting degree increases. This is supported by the high FeO and TiO<sub>2</sub> contents (Fig. 8a and Table 1) and the high CaO/Al<sub>2</sub>O<sub>3</sub> ratio (Fig. 2) of Mururoa basalts, features characteristic of melts derived from silica-deficient eclogite (Kogiso and Hirschmann, 2006; Prytulak and Elliott, 2007; Lambart et al., 2013).

In panel b of Figure 8, we compare the measured isotopic compositions of *Muru* basalts with mixing curves between depleted peridotite and the eclogitic material determined by Delavault et al. (2015). The isotopic change over time from Mururoa to Gambier could easily be explained by dilution of the eclogite-derived melts in peridotitic melts, associated with a decrease of the abundance of sedimentary material in the eclogitic component (Fig. 8b). However, the presence of continental sediments in the eclogite drastically decreases Ce/Pb in eclogite (Ce/Pb  $\approx$  11 assuming 3% sediment in eclogite; diamond symbols in Fig. 8c). Considering the range of Ce/Pb ratios of *Muru* lavas (20 – 35, Fig. 8c) the presence of continental sediments in the source of the *Muru* group must therefore be excluded.

We explore below how such sediment-free eclogite in the source region could explain the isotopic and trace-element composition of *Muru* basalts. One strong constraint comes from the Nd-Hf array of *Muru* basalts in Figure 4b that extends to Hf values almost as low as those observed in HIMU basalts. This suggests that the eclogite should have evolved with similar Sm/Nd and Lu/Hf and be as old as the source of HIMU basalts. *Muru* basalts should not, therefore, be considered as young-HIMU basalts (Thirlwall, 1997; Vidal, 1992). In the panel c of Figure 8, we show the Ce/Pb and <sup>176</sup>Hf/<sup>177</sup>Hf ratios predicted for melts formed by 1 to 10% melting of a source region consisting in depleted peridotite and pure basaltic crust. The decrease of Ce/Pb with increasing <sup>176</sup>Hf/<sup>177</sup>Hf from Mururoa to some Gambier basalts can be explained by the progressive dilution of the eclogite-derived melt with increasing melting degree, even if the model fails to reproduce the composition of some Gambier basalts (see Fig. 8 caption for details).

The old recycled oceanic crust in the *Muru* source should have developed radiogenic Pb isotopes, but *Muru* basalts have much lower Pb isotope ratios than HIMU (see Figs 4c and d). One solution would be that the recycled crust had much lower U/Pb ( $\mu$ ) and Th/U ( $\kappa$ ) ratios than the classical HIMU source. Given that the *Muru* basalts have high Ce/Pb (Fig. 5c) probably due to a preferential Pb loss during subduction processes (Table S7), the low  $\mu$  and  $\kappa$  in the eclogite would then require much lower U and Th contents in the eclogite than in N-MORB. E-MORB do not fulfill the criteria (Table S9; see also the E-MORB curve in Fig. 7b) but D-MORB or oceanic gabbros could be suitable candidates as they have low  $\mu$  (7.9 and 4.5, respectively; see Table S9 for D-MORB and Stracke et al., 2003 for gabbros). Yet, they also have significantly lower  $^{87}\text{Rb}/^{87}\text{Sr}$  ratios than DMM (0.027 for D-MORB and 0.006 for gabbros versus 0.056 for DMM; Table S9) and, it would then be expected that the Mururoa basalts have lower  $^{87}\text{Sr}/^{86}\text{Sr}$  ratios than the Gambier lavas, contrary to the trend observed in Figure 4a. Alternatively, the eclogite recycled into the *Muru* source region could have lost during subduction a significant fraction of not only its Pb but also its U and Th so that the increase of  $\mu$  and  $\kappa$  remains moderate. In Figure 8d, we show the range of  $^{206}\text{Pb}/^{204}\text{Pb}$  and  $^{207}\text{Pb}/^{204}\text{Pb}$  of eclogite-bearing materials with ages between 1.5 and 2 Gy and  $\mu$  values calculated using the mobility coefficients of Pb and U listed in Table S9. The range of  $^{206}\text{Pb}/^{204}\text{Pb}$  of *Muru* basalts is successfully reproduced, whatever the age is, for a proportion of eclogite-derived melts between 15 and 75%. However, the modeled  $^{207}\text{Pb}/^{204}\text{Pb}$  ratio is systematically higher than observed (Fig. 8d). This offset cannot be explained by a poor estimate of U and Pb contents in the eclogite, as the radiogenic production of  $^{206}\text{Pb}$  and  $^{207}\text{Pb}$  are both linked to the same U/Pb ratio. A younger age of the eclogite would improve the fit but as mentioned above, it is incompatible with the low Hf isotope ratios of the extreme Mururoa basalts (Fig. 8c), which require an old age. This suggests that the misfit between mixing curves and data in Figure 8d comes from the composition assumed for the depleted

end-member of the mixing array. As an alternative to DMM, we calculated the Pb isotope array between old eclogite and an ambient mantle similar to the PLUME end-member identified at Hawaii and Galàpagos by Nobre Silva et al. (2013) and Harpp and Weis (2020). This PLUME component is more enriched than DMM (Fig. 7 and Table S9) and its composition is globally close to that of FOZO (FOcus ZOne; Hart et al., 1992), C (Common component; Hanan and Graham, 1996), or PREMA (PREvalent MAntle; Zindler and Hart, 1986). Harpp et al. (2020) provided some constraints on its trace-element composition (Table S9), allowing quantification of our model. Figure 8d shows that the range of  $^{206}\text{Pb}/^{204}\text{Pb}$  and  $^{207}\text{Pb}/^{204}\text{Pb}$  ratios in *Muru* basalt overlaps with a mixing array between PLUME and eclogite sources, using ages of 1.5 to 2 Gy and a  $\mu$  value of 19 for the eclogite (multiple solutions can, however, be found). Assuming as Hart et al. (1992) and Harpp and Weis (2020) that PLUME/FOZO component may represent lower mantle entrained into the plumes, our result suggest that the Pacific lower mantle could constitute the ambient mantle of the *Muru* source region, as in Hawaii and Galàpagos.

The best interpretation is therefore that the source region of the *Muru* group contains at minima 5% of old sediment-free eclogite, as constrained by the olivine data of Gambier basalts (Delavault et al., 2015), and up to 95% of ambient mantle possibly similar to the Pacific lower mantle but certainly different from DMM. The isotopic compositions of *Muru* melts then depend on the melting degree, with the low-degree melts sampled at Mururoa having the highest imprint of eclogite.

### 5.3 Origin of the low $\text{Nb}_\text{N}/\text{Nb}^*$ *Pitis* and Society basalts

The low  $\text{Nb}_\text{N}/\text{Nb}^*$  and Ce/Pb ratios in *Pitis* and Society basalts rule out an overwhelming contribution of mafic crust in their mantle source region (Figs 5c-d), as is the

case for the *Muru* group, and rather point toward the involvement of continental material, as suggested in the past (e.g., Dupuy et al., 1989; Chauvel et al., 1992; Hémond et al., 1994; White and Duncan, 1996; Dostal et al., 1998; Eisele et al., 2002; Honda and Woodhead, 2005). The  $Nb_N/Nb^*$  and Ce/Pb ratios decrease with increasing  $^{87}Sr/^{86}Sr$  as shown in Figures 6a and c, indicating we can use the  $Nb_N/Nb^*$  ratio as a proxy for the contribution of continental material and we can examine the relationships between  $Nb_N/Nb^*$ , other trace-element ratios and isotope ratios to evaluate how the continental material in the *Pitis* and Society mantle source regions differ.

Most incompatible trace-element ratios are similar in *Pitis* group and Society chain; this is the case for example for La/Th, Th/U, Nb/Ta, Zr/Sm (Table S1). The only exception is the low Ba/La ratio in *Pitis* basalts compared with Society basalts (Fig. 5b). Such low Ba/La ratio is not consistent with a lower continental crust origin for *Pitis* basalts, because lower crust has higher Ba/La than other continental reservoirs (Fig. 5d and Table S7). We note, however, that *Pitis* basalts have much lower Ba/La ratios than other EM1 basalts ( $< 9.5$  versus  $\sim 12$ , Tables 1 and 2) and the observations made from *Pitis* basalts might not apply to other EM1 basalts such as those of Walvis Ridge or Tristan de Cunha. The  $Eu_N/Eu^*$  ratio ( $Eu^* = (Sm_N \times Gd_N)^{1/2}$ ) – used as a proxy for the involvement of lower crust in the mantle source region of Tristan de Cunha basalts by Willbold and Stracke (2010) – does not add much to the discussion, because it decreases at  $MgO < 7$  wt.% in *Pitis* lavas (Fig. S6d), indicating it has been modified by plagioclase fractionation and is not a source ratio.

*Pitis* and Society basalts are indistinguishable in  $^{87}Sr/^{86}Sr$  -  $Nb_N/Nb^*$  space (Fig. 6a) while they define two distinct trends when other isotope ratios are plotted versus  $Nb_N/Nb^*$  (Figs 6b-d): at any given  $Nb_N/Nb^*$  value, the *Pitis* group has lower  $^{143}Nd/^{144}Nd$ ,  $^{176}Hf/^{177}Hf$  and Pb isotopes than the Society basalts. More remarkably, while the  $^{208}Pb^*/^{206}Pb^*$  ratio ( $^{208}Pb^*/^{206}Pb^* = [^{208}Pb/^{204}Pb - 29.475]/[^{206}Pb/^{204}Pb - 9.307]$ , Galer and O’Nions, 1985) is

roughly constant in Society basalts, this ratio negatively correlates with  $Nb_N/Nb^*$  in the *Pitis* group, where it reaches extremely high values (up to 1.15, Fig. 6d), values not matched by any other OIB. We also note that  $^{87}Sr/^{86}Sr$  reaches higher values in *Pitis* basalts than in other EM1 lavas, while  $^{143}Nd/^{144}Nd$ ,  $^{176}Hf/^{177}Hf$  and  $^{206}Pb/^{204}Pb$  are distinctly lower (Fig. 4). This strengthens the observation that the enriched material in the *Pitis* source region is unique and its origin might not be extrapolated to other EM1-flavored mantle domains.

Differences of radiogenic isotopes between the most enriched compositions in *Pitis* and Society groups can result from different time-integrated parent-daughter ratios and/or different ages of the enriched material present in the source region. On the other hand, the less enriched compositions along the *Pitis* and Society arrays result from a higher proportion of ambient mantle and/or oceanic crust in the source region or participating to melting. We calculated the  $Nb_N/Nb^*$  and Nd-Hf isotopic ratios of various recycled materials, including oceanic crust and a range of sediments - of distinct origin and age, and we compare these compositions with *Pitis* and Society lavas in Figure 9. The involvement of terrigenous sediments and oceanic crust in the Society mantle source region can reasonably reproduce the lowest  $^{143}Nd/^{144}Nd$  and  $^{176}Hf/^{177}Hf$  ratios of Society basalts, as suggested in the past (Hémond et al., 1994; White and Duncan, 1996; Cordier et al., 2016). Figure 9a shows as an example the case of material recycled at 1.5 Gy, a mixture that reproduces the most enriched compositions. Additional constraints are given by the  $^{176}Hf/^{177}Hf$  versus  $Nb_N/Nb^*$  relationship (Fig. 9b), which shows the composition of recycled oceanic crust and sediments and their mixing arrays. Along these arrays, the  $Nb_N/Nb^*$  ratio of the recycled material decreases at almost constant  $^{176}Hf/^{177}Hf$  as long as the proportion of sediments is less than 10%. By contrast, mixing any recycled material with depleted mantle results in sub-vertical arrays. The almost horizontal field defined by Society lavas in Figure 9b suggests that an important part

of the variability comes from varying proportion of recycled oceanic crust and sediments, while differences of proportions of depleted ambient mantle play a smaller role.

The case is clearly more complex for the *Pitis* group with its lower Hf isotopes and its steeper slope in Figure 9b. No simple combination of continental reservoirs can successfully replicate the trace-element and isotopic differences observed between the enriched ends of *Pitis* and Society groups. A major constraint on the *Pitis* source region comes from the observation that the enriched material must have very high Th/U and be very old to reach its extreme  $^{208}\text{Pb}^*/^{206}\text{Pb}^*$  ratios. Ancient age is supported by the study of Delavault et al. (2016) who identified sulfides with negative mass-independent fractionation of S isotopes in some *Pitis* lavas, requiring that the source region contains Archean material. On the other hand, high Th/U in modern continental material is only observed in pelagic clays (Th/U = 8, Table S7), and to a lesser extent in the lower crust (Th/U = 6; Rudnick and Gao, 2003). We showed, however, that involvement of lower crust in the *Pitis* mantle source region is unlikely, due to the observed low Ba/La ratios of lavas. Pelagic clays have high Lu/Hf and Rb/Sr ratios while having the same Sm/Nd ratio as other continental materials (Table S9). Over time, pelagic clays recycled into the mantle will acquire high  $^{176}\text{Hf}/^{177}\text{Hf}$  and  $^{87}\text{Sr}/^{86}\text{Sr}$  but will have the same  $^{143}\text{Nd}/^{144}\text{Nd}$  as other continent-derived material (Fig. 7a). As a consequence, if the recycled material in the *Pitis* source region included pelagic clays, we would expect the *Pitis* group to plot above the Society group in Figure 6a and c, but it is not the case. However, since Sr isotopes strongly depend on the proportion of continental materials in the mantle source region – in addition to their nature, a slight difference in their contribution to the melts could explain the difference between the extreme *Pitis* and Society basalts. By contrast,  $^{143}\text{Nd}/^{144}\text{Nd}$  and  $^{176}\text{Hf}/^{177}\text{Hf}$  isotope ratios are far less dependent on sediment/oceanic crust/depleted mantle proportions (Table S9). Their relative behavior is a more robust tool to determine the origin of the continental material. Figure 9 demonstrates that mixing 2.5 Gy

pelagic clays with oceanic crust cannot produce the low  $^{176}\text{Hf}/^{177}\text{Hf}$  ratios of the most extreme *Pitis* lavas. A sand/pelagic clay mixture, as suggested by Eisele et al. (2002), could potentially explain the  $\text{Nb}_\text{N}/\text{Nb}^*$ -Hf isotope relationship shown in Figure 9 but it would require an age older than 2.5 Ga. Alternatively, the enriched material in the *Pitis* source could resemble Archean cherts or carbonates, as proposed by Delavault et al. (2016) and Wang et al. (2018), but our combined geochemical and isotopic data do not add much in favor or against these models (Fig. 9). The origin of the continental material incorporated into the *Pitis* source thus remains unclear but the isotopic characteristics suggest that it is old, possibly Archean, and it has a high Th/U to account for the elevated  $^{208}\text{Pb}^*/^{206}\text{Pb}^*$  ratios coupled to a low Lu/Hf ratio to reproduce the low  $^{176}\text{Hf}/^{177}\text{Hf}$  of *Pitis* lavas compared to other OIB. Finally, within the *Pitis* group, we observe that, with increasing  $\text{Nb}_\text{N}/\text{Nb}^*$ ,  $^{176}\text{Hf}/^{177}\text{Hf}$  progressively increases while alkalinity,  $(\text{La}/\text{Sm})_\text{N}$ ,  $^{87}\text{Sr}/^{86}\text{Sr}$  and  $^{208}\text{Pb}^*/^{206}\text{Pb}^*$  decrease from Pitcairn Island to Pitcairn Seamounts (Figs 6 and S8). This evolution is not consistent with varying proportion of sediment and crust in the recycled material (Fig. 9b) but rather suggests that the contribution of the recycled material decreases through time, due to the progressive increase of the extent of melting and a larger proportion of ambient mantle contributing to the isotopic composition of melts.

In summary, most of the isotopic variability of the Society group is explained by a changing proportion of sediments to oceanic crust in the recycled material, but it is not the case for the *Pitis* group. The oblique array formed by *Pitis* lavas in the  $^{176}\text{Hf}/^{177}\text{Hf}$  versus  $\text{Nb}_\text{N}/\text{Nb}^*$  diagram of Figure 9b is best explained by a growing contribution of the ambient mantle, which could be the FOZO/PLUME mantle identified in the *Muru* group.

#### 5.4 Geochemical constraints on the internal structure of the two plumes

The variations observed for very incompatible trace-element and isotope ratios through time and along the two Polynesian island chains show contrasting patterns that suggest different distribution of the recycled material within the plume. Along the Society chain, the ranges of  $Nb_N/Nb^*$  and Ce/Pb known for each island almost cover the ranges known for the entire chain (Figs 5 and 6), as observed for radiogenic isotopes in Figure 10a (see also Cordier et al., 2016). As a consequence, the relative contribution of continental sediments, oceanic crust and depleted mantle to the isotopic composition of Society lavas varies significantly during the construction of individual islands. This implies that their volumes are small compared to the source region of each volcano and randomly distributed within the central part of the plume stem (Fig. 10c). Whether they are concentrically zoned or not in the plume stem (White and Duncan, 1996; Cordier et al., 2005) cannot be evaluated since we deliberately disregarded the post-shield lavas in our dataset. On a longer timescale, that of the archipelago (5 My), no specific geochemical evolution is seen (Fig. 10a), suggesting that the heterogeneities are evenly distributed within the plume and that the enriched materials spread vertically over hundred of kilometers to form filament-like heterogeneities within the plume stem (Fig. 10c; Farnetani et al., 2018).

In contrast to the Society chain, two groups of volcanoes can be identified along the Pitcairn-Gambier volcanic alignment based on basalt geochemistry and origin of the material recycled in the plume region. The oldest volcanoes (5 to 12 My, Mururoa and Fangataufa atolls and Gambier Island) derive from melting of ambient mantle, possibly similar to the Pacific lower mantle, and old oceanic crust converted into eclogite. In the group, over time, the eclogite-derived melts are progressively diluted with increasing melting rate as shown by changing Nd and Hf isotope ratios (Fig. 10b) and decrease of alkalinity,  $TiO_2$  and  $(La/Sm)_N$  (Figs 8a and S8). The situation changed after the formation of Gambier Island. The low  $Nb_N/Nb^*$  and isotopic compositions of the *Pitis* group (Pitcairn Island and Pitcairn

Seamounts) suggest a very different source that includes old, possibly Archean, continent-derived material with unclear origin. This source massively contributed to melting at 1 My (Pitcairn Island) before being diluted in more recent melts (Pitcairn Seamounts), as melting proceeded (Fig. 10b). In both segments of the Pitcairn-Gambier chain (*Muru* versus *Pitis*), the largest influence of the recycled components is recorded by the low-degree melts produced at Mururoa and Pitcairn Island, probably because enriched components have lower melting temperature than ambient peridotite (e.g., Batiza, 1984; Phipps Morgan and Morgan, 1999).

Incompatible-trace element and isotopic variations along the Pitcairn-Gambier chain indicate that at some time between 5 and 1 My, a sharp change of the recycled material sampled by melting occurred (Fig. 10b). We argue that this change does not result from a lithospheric thickness control on decompression melting depth (Dupuy et al., 1993), because the lithosphere thickness varies by less than 2 km between the edification of Mururoa and Pitcairn Seamounts (Dasgupta et al., 2010). We suggest that the jump from *Muru* to *Pitis* composition could result from the arrival in the melting region of discrete heterogeneities, as detected in the Canary Islands by Taylor et al. (2017, 2020). Between 12 and 5 My, only eclogite was present in the melting region to form the *Muru* group of lavas; at some time during the past 5 My, Archean sediments entered the melting region (Fig. 10c). The transit of the eclogite across the melting zone can thus be traced from Mururoa to Gambier, i.e. during 7 My, implying eclogite has an elongated filament shape as modeled by Farnetani et al. (2018). Interestingly, Farnetani et al. (2018) showed in their Figure 5 that after their introduction in the melting zone, the volume of filament-like heterogeneities decreases smoothly through time. This feature could explain the isotopic arrays observed in the *Muru* group, with a significant decrease of the eclogite imprint through time. The jump to the *Pitis* composition occurred at some time between 5 and 1 My but its exact timing is still

unconstrained by lack of samples from seamounts located between Gambier and Pitcairn Islands (Fig. 1a).

In Figure 10c, we schematically synthesize the way crustal components might occur in the mantle dome beneath Polynesia. We combine our results with those known for the Marquesas chain and for the last 20 My of the Cook-Austral chains (Cook-Austral and Arago volcanic lineaments). Isotopic changes along the Cook-Austral chains are shown in Figure S10; for the variations along the Marquesas chain the reader can refer to Figure 11 of Chauvel et al. (2012). The first important observation is that each Polynesian plume defines its own trend in isotopic spaces, showing that the heterogeneities contained in the dome are very diverse in origin and age (Kogiso, 2013; Chauvel et al., 2014), as illustrated by the different colors in Figure 10c. Importantly, the spatial and temporal patterns of the isotopic variations in each Polynesian chain also suggest that the heterogeneities are sampled by each plume, with a possible north-south dichotomy. In the southern chains, high  $Nb_N/Nb^*$  melts occur over millions of years in the oldest HIMU islands of the Cook-Austral chain (Vidal et al., 1984; Chauvel et al., 1992; Hémond et al., 1994; Woodhead 1996), just like in the *Muru* group of Pitcairn-Gambier chain (Fig. 10b). The time evolution of both chain is also similar: in the Pitcairn-Gambier chain, a continental component appears after 5 My to form the *Pitis* group and along the Cook-Austral, the early HIMU signature of Mangaia, Tubuai and old-Rurutu lavas is replaced around 6 My by compositions indicating an increased proportion of sediments to melting (Fig. S10; Hémond et al., 1994; Woodhead, 1996; Jackson et al., 2020). Jackson et al. (2020) link these isotopic variations to the position of volcanoes along the chain and to a control of the lithospheric thickness on melt composition, but our results on the Pitcairn-Gambier chain do not favor such interpretation because the variation in lithospheric thickness is minor. We suggest that the isotopic change arises from the presence of successive filaments with different compositions into the melting region. The same interpretation could

also apply to the Arago plume (which forms part of the Cook-Austral chains), in which HIMU-like material (Chauvel et al., 1997; Jackson et al., 2020) would have succeeded 3 My ago to a sediment-dominated filament in the melting region (Fig. S10). We envision therefore that filaments of distinct compositions are vertically successive within these three plume stems (Fig. 10c).

In the northern Society and Marquesas chains, the imprint of continental sediments is continuous for the last 5.5 My. Such difference in pattern between northern and southern hotspots could simply result from the relatively recent and short magmatic activity of both Society and Marquesas plumes (< 6 My), compared to the time it takes for filaments, hundreds of kilometers long, to transit across the melting region (> 4 My; Farnetani et al., 2018). It could, however, also reveal a different distribution of heterogeneities in the southern and northern parts of the Polynesian dome.

We have demonstrated above that the nature of the enriched materials present in the Polynesian plume stems does not vary over a period of up to 6 My, which suggests the predominance of filament-shaped heterogeneities in the Polynesian plumes, regardless of their composition. This can be explained by the rheological behavior of heterogeneities during plume ascent, as predicted by Farnetani et al. (2018): the viscosity of the enriched materials in the Polynesian plumes would have to be very high (30 times that of the surrounding mantle) to prevent chemical heterogeneities to develop filament-like shape during their deformation in the rising plumes. Nevertheless, the geometry of heterogeneities in the plume stems cannot solely explain the amplitude of the isotopic variations in island chains (Farnetani et al., 2018): Hawaii and Polynesian plumes all contain filament-like enriched domains, but the isotopic variability recorded in Hawaii is far less important than in Polynesian plumes (see the Figure 12 in Chauvel et al., 2012) and the role of melt production rate has to be taken into account (Chauvel et al., 2012). Weak plumes, such as the Polynesian ones, produce melts by relatively

low melting degrees and in these circumstances, the isotopic diversity of the mantle plume region is more likely preserved in the erupted lavas.

## 6. Conclusion

Using incompatible trace-element ratios ( $Nb_N/Nb^*$ , Ce/Pb and Ba/La) and isotope ratios of the Pitcairn-Gambier and Society Island basalts in French Polynesia, we examine the similarities and differences between the two plume sources and the consequences relative to their potential origin.

In the Society chain, the mantle source region displays the typical fingerprint of continental material with low  $Nb_N/Nb^*$  and Ce/Pb and elevated  $^{87}Sr/^{86}Sr$ . As widely accepted, it most probably incorporates terrigenous sediments, but the age of this material is still undetermined. Lavas from individual islands show almost the entire geochemical range known for the entire archipelago and no systematic evolution occurs during the edification of the chain. This suggests that enriched domains are randomly distributed within the plume and form filaments that spread vertically over thousands of kilometers.

Along the Pitcairn-Gambier chain, a clear geochemical dichotomy exists between old (*Muru* group: Mururoa, Fangataufa, Gambier, > 5 My) and recent volcanoes (*Pitis* group: Pitcairn Island and Seamounts, <1 My). Lavas from the *Muru* group have high  $Nb_N/Nb^*$  and Ce/Pb and they define a steep trend that extends below the mantle array in the Nd-Hf isotopic space: the presence of old eclogite in their mantle source region could explain the observed features. The unradiogenic Pb isotope ratios of *Muru* lavas are therefore puzzling and can neither be explained by the addition of sediments (it would have decreased Ce/Pb), nor by a young age of the eclogite (it would have increased  $^{176}Hf/^{177}Hf$ ), nor by removal of U during subduction (it would not fit with the  $^{206}Pb/^{204}Pb - ^{207}Pb/^{204}Pb$  relationship). We conclude that

mixing of old eclogite-derived melts with melts derived from an ambient mantle more enriched than DMM and potentially similar to the PLUME/FOZO mantle component. In contrast, the *Pitis* lavas have much more enriched compositions, with  $Nb_N/Nb^*$  as low and  $^{87}Sr/^{86}Sr$  almost as high as Society lavas, consistent with the presence of continental material in their mantle source region. Although the *Pitis* enriched material is generally considered to be an archetype for EM1 sources, this continental component is nevertheless unique. It has low Ba/La,  $^{143}Nd/^{144}Nd$  and  $^{176}Hf/^{177}Hf$  and exceptionally high  $^{208}Pb^*/^{206}Pb^*$  compared to worldwide OIB. The origin of this very old material, possibly Archean, remains enigmatic because terrigenous sediments have too low Th/U, lower continental crust has too high Ba/La and pelagic clays have too high Lu/Hf to account for the trace-element and isotopic compositions of *Pitis* lavas. Finally, the geochemical dichotomy observed along the Pitcairn-Gambier chain calls for the successive introduction into the melting region of distinct filament-like heterogeneities. Sampling of seamounts located between *Muru* and *Pitis* volcanoes would provide access to the transition between the two sources and would allow a better picture of the long-term behavior structure of the Pitcairn-Gambier plume.

When placed in the more general frame of Polynesian plume magmatism, the results obtained at Society and Pitcairn-Gambier demonstrate the complex nature and distribution of materials present in the Polynesian dome and suggest accumulation and sampling of materials with diverse ages and nature in the same large and deep structure of the Earth's mantle.

### **Acknowledgments**

We thank S. Bureau, S. Campillo, P. Telouk and P. Nonnotte for their help during analytical work. We are grateful to C. Hémond for the sharing of some trace-element data on the island of Moorea included in this study. We would like also to thank the AE R. Hickey-

Vargas and the three anonymous reviewers for their helpful and detailed reviews that greatly enhanced the quality and implications of this manuscript. This study was financially supported by the ANR grant “M & Ms” (ANR-10-BLAN-0603M&Ms; Mantle Melting - Measurements, Models, Mechanisms), Labex OSUG@2020 and the University Grenoble Alpes (SMINGUE Project, Earth Universe) and the ERC SHRED (grant n° 833632). This is IPGP contribution number 4186.

## References

- Achard S. (1987) Etude d'une série moyennement alcaline en contexte intra-plaque océanique: Mururoa (Polynésie française). Master Thesis, Univ. Clermont-Ferrand.
- Adam C. and Bonneville A. (2005) Extent of the South Pacific Superswell. *J. Geophys. Res.* **110**, B09408, doi: 10.1029/2004JB003465.
- Batiza R. (1984) Inverse relationship between Sr isotope diversity and rate of oceanic volcanism has implications for mantle heterogeneity. *Nature* **309**, 440–441.
- Béguelin P., Bizimis M., Beier C. and Turner S. (2017) Rift–plume interaction reveals multiple generations of recycled oceanic crust in Azores lavas. *Geochim. Cosmochim. Acta* **218**, 132–152.
- Binard N. (1991) Les points chauds de la Société, des Australes et de Pitcairn (Pacifique Sud): Approche volcanologique et pétrologique. Ph.D. Thesis, Univ. Bretagne Occidentale.
- Binard N., Maury R. C., Guille G., Talandier J., Gillot P. Y. and Cotten J. (1993) Mehetia Island, South Pacific: geology and petrology of the emerged part of the Society hot spot. *J. Volcanol. Geotherm. Res.* **55**, 239–260.
- Blais S., Guille G., Guillou H., Chauvel C., Maury R. C. and Caroff M. (2000) Geology, geochemistry and geochronology of Bora Bora island (Society islands, French Polynesia).

*CR. Acad. Sci. II A* **331**, 579–585.

Blais S., Guille G., Guillou H., Chauvel C., Maury R. C., Pernet G. and Cotten J. (2002) The island of Maupiti: the oldest emergent volcano in the Society hot spot chain (French Polynesia). *B. Soc. Geol. Fr.* **173**, 45–55.

Blais S., Maury R. C., Guille G. and Guillou H. (2004) *Carte géologique de Raiatea-Tahaa, Polynésie Française (1/100 000), notice explicative*. Bureau de Recherche Géologique et Minière, Orléans.

Blais S., Maury R. C., Guille G. and Guillou H. (2006) *Carte géologique de Bora-Bora/Maupiti, Polynésie Française (1/30 000), notice explicative*. Bureau de Recherche Géologique et Minière, Orléans.

Boyet M., Doucelance R., Israel C., Bonnand P., Auclair D., Suchorski K. and Bosq C. (2019) New Constraints on the Origin of the EM-1 Component Revealed by the Measurement of the La-Ce Isotope Systematics in Gough Island Lavas. *Geochem. Geophys. Geosyst.* **20**, 2484–2498, doi: 10.1029/2019GC008228.

Buff L., Jackson M. G., Konrad K., Konter J. G., Bizimis M., Price A., Rose-Koga E. F., Blusztajn J., Koppers A. A. P. and Herrera S. (2021) “Missing links” for the long-lived Macdonald and Arago hotspots, South Pacific Ocean. *Geology* **49**, doi:10.1130/G48276.1.

Caroff M. (1992) *Géochimie et pétrologie des roches volcaniques des forages d’Eiao et de Mururoa (Polynésie française): approche des processus de genèse et d’évolution des magmas basaltiques en contexte intraplaque océanique*. Ph.D. Thesis, Univ. Bretagne Occidentale.

Caroff M., Maury R. C., Guille G., Bellon H. and Cotten J. (1993) Les basaltes de l’Archipel des Gambier (Polynésie française). *CR. Acad. Sci. II A* **317**, 359–366.

Chauvel C. and Blichert-Toft J. (2001) A hafnium isotope and trace element perspective on melting of the depleted mantle. *Earth Planet. Sci. Lett.* **190**, 137–151.

- Chauvel C., Hofmann A. W. and Vidal P. (1992) HIMU-EM: The French Polynesian connection. *Earth Planet. Sci. Lett.* **110**, 99–119.
- Chauvel C., McDonough W., Guille G., Maury R. C. and Duncan R. (1997) Contrasting old and young volcanism in Rurutu Island, Austral chain. *Chemical Geology* **139**, 125–143.
- Chauvel C., Lewin E., Carpentier M., Arndt N. and Marini J.-C. (2008) Role of recycled oceanic basalt and sediment in generating the Hf–Nd mantle array. *Nat. Geosci.* **1**, 64–67.
- Chauvel C., Bureau S. and Poggi C. (2011) Comprehensive chemical and isotopic analyses of basalt and sediment reference materials. *Geostand. Geoanal. Res.* **35**, 125–143.
- Chauvel C., Maury R. C., Blais S., Lewin E., Guillou H., Guille G., Rossi P. L. and Gustscher M.-A. (2012) The size of plume heterogeneities constrained by Marquesas isotopic stripes. *Geochem. Geophys. Geosyst.* **13**, Q07005, doi: 10.1029/2012GC004123.
- Chauvel C., Delavault H. and Cordier C. (2014) Polynesia: a weak and disorganized superplume. *Goldschmidt Conference #388* (abstr.).
- Cordier C., Clément J.-P., Caroff M., Hémond C., Blais S., Cotten J., Bollinger C., Launeau P. and Guille G. (2005) Petrogenesis of coarse-grained intrusives from Tahiti-Nui and Raiatea (Society Islands, French Polynesia). *J. Petrol.* **46**, 2281–2312.
- Cordier C., Chauvel C. and Hémond C. (2016) High-precision lead isotopes and stripy plumes: Revisiting the Society chain in French Polynesia. *Geochim. Cosmochim. Acta* **189**, 236–250.
- Courtillot V., Davaille A., Besse J. and Stock J. (2003) Three distinct types of hotspots in the Earth's mantle. *Earth Planet. Sci. Lett.* **205**, 295–308.
- Dasgupta R., Jackson M. G. and Lee C.-T. A. (2010) Major element chemistry of ocean island basalts — Conditions of mantle melting and heterogeneity of mantle source. *Earth Planet. Sci. Lett.* **289**, 377–392.
- Davaille A. (1999) Simultaneous generation of hotspots and superswells by convection in

a heterogeneous planetary mantle. *Nature* **402**, 756–760.

Delavault H., Chauvel C., Sobolev A. and Batanova V. (2015) Combined petrological, geochemical and isotopic modeling of a plume source: Example of Gambier Island, Pitcairn chain. *Earth Planet. Sci. Lett.* **426**, 23–35.

Delavault H., Chauvel C., Thomassot E., Devey C. W. and Dazas B. (2016) Sulfur and lead isotopic evidence of relic Archean sediments in the Pitcairn mantle plume. *Proc. Natl. Acad. Sci. USA* **113**, 12952.

Devey C. W., Lackschewitz K., Mertz D. F., Bourdon B., Cheminée J. L., Dubois J., Guivel C., Hékinian R. and Stoffers P. (2003) Giving birth to hotspot volcanoes: Distribution and composition of young seamounts from the seafloor near Tahiti and Pitcairn islands. *Geology* **31**, 395–398.

Dostal J., Cousens B. and Dupuy C. (1998) The Incompatible Element Characteristics of an Ancient Subducted Sedimentary Component in Ocean Island Basalts from French Polynesia. *J. Petrol.* **39**, 937–952.

Duncan R. A. and McDougall I. (1976) Linear volcanism in French Polynesia. *J. Volcanol. Geotherm. Res.* **1**, 197–227.

Duncan R. A., McDougall I., Carter R. M. and Coombs D. S. (1974) Pitcairn Island—another Pacific hot spot? *Nature* **251**, 679–682.

Dupuy C., Barszczus H. G., Dostal J., Vidal P. and Liotard J.-M. (1989) Subducted and recycled lithosphere as the mantle source of ocean island basalts from southern Polynesia, central Pacific. *Chem. Geol.* **77**, 1–18.

Dupuy C., Vidal P., Maury R. C. and Guille G. (1993) Basalts from Mururoa, Fangataufa and Gambier islands (French Polynesia): Geochemical dependence on the age of the lithosphere. *Earth Planet. Sci. Lett.* **117**, 89–100.

Eisele J., Sharma M., Galer S. J. G., Blichert-Toft J., Devey C. W. and Hofmann A. W.

(2002) The role of sediment recycling in EM-1 inferred from Os, Pb, Hf, Nd, Sr isotope and trace element systematics of the Pitcairn hotspot. *Earth Planet. Sci. Lett.* **196**, 197–212.

Farnetani C. G., Hofmann A. W., Duvernay T. and Limare A. (2018) Dynamics of rheological heterogeneities in mantle plumes. *Earth Planet. Sci. Lett.* **499**, 74–82.

French S. W. and Romanowicz B. A. (2015) Broad plumes rooted at the base of the Earth's mantle beneath major hotspots. *Nature* **525**, 95–99.

Gale A., Dalton C. A., Langmuir C. H., Su Y. and Schilling J.-G. (2013) The mean composition of ocean ridge basalts. *Geochem. Geophys. Geosyst.* **14**, 489–518, doi: 10.1029/2012GC004334.

Galer S. J. G. and O'Nions R. K. (1985) Residence time of thorium, uranium and lead in the mantle with implications for mantle convection. *Nature* **316**, 778–782.

Garapić G., Jackson M. G., Hauri E. H., Hart S. R., Farley K. A., Blusztajn J. S. and Woodhead J. D. (2015) A radiogenic isotopic (He-Sr-Nd-Pb-Os) study of lavas from the Pitcairn hotspot: Implications for the origin of EM-1 (enriched mantle 1). *Lithos* **228–229**, 1–11.

Gillot P.-Y., Cornette Y. and Guille G. (1992) Age (K-Ar) et conditions d'édification du soubassement volcanique de l'atoll de Mururoa (Pacifique Sud). *CR. Acad. Sci. II A* **314**, 393–399.

Guillou H. (1990) Le soubassement volcanique de l'atoll de Fangataufa (Polynésie Française), géologie et pétrologie. Ph.D. Thesis, Univ. Paris Sud.

Guillou H., Guille G., Brousse R. and Bardintzeff J. M. (1990) Evolution de basaltes tholeiitiques vers des basaltes alcalins dans le substratum volcanique de Fangataufa (Polynésie française). *B. Soc. Geol. Fr.* **6**, 537–549.

Hanan B. B. and Graham D. W. (1996) Lead and Helium Isotope Evidence from Oceanic Basalts for a Common Deep Source of Mantle Plumes. *Science* **272**, 991–995.

Hanyu T., Tatsumi Y., Senda R., Miyazaki T., Chang Q., Hirahara Y., Takahashi T., Kawabata H., Suzuki K., Kimura J.-I. and Nakai S. (2011) Geochemical characteristics and origin of the HIMU reservoir: A possible mantle plume source in the lower mantle. *Geochem. Geophys. Geosyst.* **12**, Q0AC09, doi: 10.1029/2010GC003252.

Harpp K. S. and Weis D. (2020) Insights Into the Origins and Compositions of Mantle Plumes: A Comparison of Galápagos and Hawai'i. *Geochem. Geophys. Geosyst.* **21**, e2019GC008887, doi: 10.1029/2019GC008887.

Hart S. R. (1988) Heterogeneous mantle domains: signatures, genesis and mixing chronologies. *Earth Planet. Sci. Lett.* **90**, 273–296.

Hart S. R., Hauri E. H., Oschmann L. A. and Whitehead J. A. (1992) Mantle plumes and entrainment: isotopic evidence. *Science* **256**, 517–520.

Hauri E. H. and Hart S. R. (1993) Re-Os isotope systematics of HIMU and EMII oceanic island basalts from the south Pacific Ocean. *Earth Planet. Sci. Lett.* **114**, 353–371

Hékinian R., Cheminée J. L., Dubois J., Stoffers P., Scott S., Guivel C., Garbe-Schönberg D., Devey C., Bourdon B., Lackschewitz K., McMurtry G. and Le Drezen E. (2003) The Pitcairn hotspot in the South Pacific: distribution and composition of submarine volcanic sequences. *J. Volcanol. Geotherm. Res.* **121**, 219–245.

Hémond C., Devey C. W. and Chauvel C. (1994) Source compositions and melting processes in the Society and Austral plumes (South Pacific Ocean): Element and isotope (Sr, Nd, Pb, Th) geochemistry. *Chem. Geol.* **115**, 7–45.

Herzberg C., Cabral R. A., Jackson M. G., Vidito C., Day J. M. D. and Hauri E. H. (2014) Phantom Archean crust in Mangaia hotspot lavas and the meaning of heterogeneous mantle. *Earth Planet. Sci. Lett.* **396**, 97–106.

Hofmann A. W. (2014) 3.3 - Sampling Mantle Heterogeneity through Oceanic Basalts: Isotopes and Trace Elements. In *Treatise on Geochemistry (Second Edition)* (eds. H. D.

Holland and K. K. Turekian). Elsevier, Oxford. pp. 67–101.

Hofmann A. W. (1997) Mantle geochemistry: the message from oceanic volcanism. *Nature* **385**, 219–229.

Hofmann A. W., Jochum K. P., Seufert M. and White W. M. (1986) Nb and Pb in oceanic basalts: new constraints on mantle evolution. *Earth Planet. Sci. Lett.* **79**, 33–45.

Honda M. and Woodhead J. D. (2005) A primordial solar-neon enriched component in the source of EM-I-type ocean island basalts from the Pitcairn Seamounts, Polynesia. *Earth Planet. Sci. Lett.* **236**, 597–612.

Ito G. and Mahoney J. J. (2005) Flow and melting of a heterogeneous mantle: 1. Method and importance to the geochemistry of ocean island and mid-ocean ridge basalts. *Earth Planet. Sci. Lett.* **230**, 29–46.

Jackson M. G., Halldórsson S. A., Price A., Kurz M. D., Konter J. G., Koppers A. A. P. and Day J. M. D. (2020) Contrasting Old and Young Volcanism from Aitutaki, Cook Islands: Implications for the Origins of the Cook–Austral Volcanic Chain. *J. Petrol.* **61**, egaa037, doi: 10.1093/petrology/egaa037.

Jochum K. P., Wilson S. A., Abouchami W., Amini M., Chmeleff J., Eisenhauer A., Hegner E., Iaccheri L. M., Kieffer B., Krause J., McDonough W. F., Mertz-Kraus R., Raczek I., Rudnick R. L., Scholz D., Steinhöfel G., Stoll B., Stracke A., Tonarini S., Weis D., Weis U. and Woodhead J. D. (2011) GSD-1G and MPI-DING Reference Glasses for In Situ and Bulk Isotopic Determination. *Geostand. Geoanal. Res.* **35**, 193–226.

Johnson M. C. and Plank T. (1999) Dehydration and melting experiments constrain the fate of subducted sediments. *Geochem. Geophys. Geosyst.* **1**, 1007, doi: 10.1029/1999GC000014.

Kogiso T. (2013) Ocean Island Basalts in Polynesia, South Pacific. *J. Geogr.* **122**, 539–545.

Kogiso T. and Hirschmann M. M. (2006) Partial melting experiments of bimineralec eclogite and the role of recycled mafic oceanic crust in the genesis of ocean island basalts. *Earth Planet. Sci. Lett.* **249**, 188–199.

Kogiso T., Tatsumi Y., Shimoda G. and Barszczus H. G. (1997) High  $\mu$  (HIMU) ocean island basalts in southern Polynesia: New evidence for whole mantle scale recycling of subducted oceanic crust. *J. Geophys. Res.* **102**, 8085–8103.

Lambart S., Laporte D. and Schiano P. (2013) Markers of the pyroxenite contribution in the major-element compositions of oceanic basalts: Review of the experimental constraints. *Lithos* **160–161**, 14–36.

Lassiter J. C., Blichert-Toft J., Hauri E. H. and Barszczus H. G. (2003) Isotope and trace element variations in lavas from Raivavae and Rapa, Cook-Austral islands: constraints on the nature of HIMU- and EM-mantle and the origin of mid-plate volcanism in French Polynesia. *Chem. Geol.* **202**, 115–138.

Le Dez A. (1996) Variations pétrologiques et géochimiques associées à l'édification des volcans-boucliers de Polynésie Française: exemples de Nuku Hiva et Hiva Oa (Marquises) et de Moorea (Société). Ph.D. Thesis, Univ. Bretagne Occidentale.

Legendre C., Maury R. C., Guillou H., Cotten J., Caroff M., Blais S. and Guille G. (2003) Geological and petrologic evolution of Huahine island (Society archipelago, French Polynesia): an unusual intraoceanic shield volcano. *B. Soc. Geol. Fr.* **174**, 115–124.

Maury R. C., Legendre C., Caroff M., Guillou H., Blais S., Chauvel C., Guille G. and Cotten J. (2001) *Carte géologique de Huahine, Polynésie Française (1/40 000), notice explicative*. Bureau de Recherche Géologique et Minière, Orléans.

McArthur J. M. (1994) Recent trends in strontium isotope stratigraphy. *Terra Nova* **6**, 331–358.

McDonough W. F. and Sun S. S. (1995) The composition of the Earth. *Chem. Geol.* **120**,

223–253.

McKenzie D. and O’Nions R. K. (1983) Mantle reservoirs and ocean island basalts.

*Nature* **301**, 229–231.

McNutt M. K. and Judge A. V. (1990) The Superswell and Mantle Dynamics Beneath the South Pacific. *Science* **248**, 969–975.

Nobre Silva I. G., Weis D. and Scoates J. S. (2013) Isotopic systematics of the early Mauna Kea shield phase and insight into the deep mantle beneath the Pacific Ocean *Geochem. Geophys. Geosyst.* **14**, 659–676, doi: 10.1002/ggge.20047.

Obayashi M., Yoshimitsu J., Sugioka H., Ito A., Isse T., Shiobara H., Reymond D. and Suetsugu D. (2016) Mantle plumes beneath the South Pacific superswell revealed by finite frequency P tomography using regional seafloor and island data. *Geophys. Res. Lett.* **43**, 11,628–11,634.

Pettke T., Kodolányi J. and Kamber B. S. (2018) From ocean to mantle: new evidence for U-cycling with implications for the HIMU source and the secular Pb isotope evolution of Earth’s mantle. *Lithos* **316–317**, 66–76.

Phipps Morgan J. (1999) Isotope topology of individual hotspot basalt arrays: Mixing curves or melt extraction trajectories? *Geochem. Geophys. Geosyst.* **1**, 1003, doi: 10.1029/1999GC000004.

Phipps Morgan J. and Morgan W. J. (1999) Two-stage melting and the geochemical evolution of the mantle: a recipe for mantle plum-pudding. *Earth Planet. Sci. Lett.* **170**, 215–239.

Plank T. (2014) The chemical composition of subducting sediments. In *Treatise on Geochemistry (2nd Edition)* (eds. H. D. Turekian and H. K.). Elsevier, Oxford. pp. 607–629.

Plank T. and Langmuir C. H. (1998) The chemical composition of subducting sediment and its consequences for the crust and mantle. *Chem. Geol.* **145**, 325–394.

- Porter K. A. and White W. M. (2009) Deep mantle subduction flux. *Geochem. Geophys. Geosyst.* **10**, Q12016, doi: 10.1029/2009GC002656.
- Prytulak J. and Elliott T. (2007) TiO<sub>2</sub> enrichment in ocean island basalts. *Earth Planet. Sci. Lett.* **263**, 388–403.
- Puckett E. G., Turcotte D. L., He Y., Lokavarapu H., Robey J. M. and Kellogg L. H. (2018) New numerical approaches for modeling thermochemical convection in a compositionally stratified fluid. *Phys. Earth Planet. Inter.* **276**, 10–35.
- Rudnick R. L. and Gao S. (2003) 3.01 - Composition of the Continental Crust. In *Treatise on Geochemistry* (eds. H. D. Holland and K. K. Turekian). Pergamon, Oxford. pp. 1–64.
- Ryan W. B. F., Carbotte S. M., Coplan J. O., O'Hara S., Melkonian A., Arko R., Weissel R. A., Ferrini V., Goodwillie A., Nitsche F., Bonczkowski J. and Zemsky R. (2009) Global Multi-Resolution Topography synthesis. *Geochem. Geophys. Geosyst.* **10**, doi:10.1029/2008GC002332.
- Salters V. J. M. and White W. M. (1998) Hf isotope constraints on mantle evolution. *Chem. Geol.* **145**, 447–460.
- Salters V. J. M. and Stracke A. (2004) Composition of the depleted mantle. *Geochem. Geophys. Geosyst.* **5**, Q05004, doi: 10.1029/2003GC000597.
- Schubert G., Masters G., Olson P. and Tackley P. (2004) Superplumes or plume clusters? *Phys. Earth Planet. Inter.* **146**, 147–162.
- Sobolev A. V., Hofmann A. W. and Nikogosian I. K. (2000) Recycled oceanic crust observed in 'ghost plagioclase' within the source of Mauna Loa lavas. *Nature* **404**, 986–990.
- Sobolev A. V., Hofmann A. W., Kuzmin D. V., Yaxley G. M., Arndt N. T., Chung S.-L., Danyushevsky L. V., Elliott T., Frey F. A., Garcia M. O., Gurenko A. A., Kamenetsky V. S., Kerr A. C., Krivolutskaya N. A., Matvienkov V. V., Nikogosian I. K., Rocholl A., Sigurdsson

I. A., Sushchevskaya N. M. and Teklay M. (2007) The amount of recycled crust in sources of mantle-derived melts. *Science* **316**, 412–417.

Stoffers P., Hékinian R. and Scientific Party of cruise SO-65 (1990) Active Pitcairn hotspot found. *Mar. Geol.* **95**, 51–55.

Stracke A., Bizimis M. and Salters V. J. M. (2003) Recycling oceanic crust: Quantitative constraints. *Geochem. Geophys. Geosyst.* **4**, 8003, doi:10.1029/2001GC000223.

Stracke A., Hofmann A. W. and Hart S. R. (2005) FOZO, HIMU, and the rest of the mantle zoo. *Geochem. Geophys. Geosyst.* **6**, Q05007, doi: 10.1029/2004GC000824.

Taylor R. N., Davila-Harris P., Branney M. J., Ruth Farley E. M., Gernon T. M. and Palmer M. R. (2020) Dynamics of a chemically pulsing mantle plume. *Earth Planet. Sci. Lett.* **537**, 116182, doi: 10.1016/j.epsl.2020.116182.

Thirlwall M. F. (1997) Pb isotopic and elemental evidence for OIB derivation from young HIMU mantle. *Chem. Geol.* **139**, 51–74.

Vervoort J. D. J. D., Plank T. and Prytulak J. (2011) The Hf–Nd isotopic composition of marine sediments. *Geochim. Cosmochim. Acta* **75**, 5903–5926.

Vidal P. (1992) Mantle: More HIMU in the future? *Geochim. Cosmochim. Acta* **56**, 4295–4299.

Vidal P., Chauvel C. and Brousse R. (1984) Large mantle heterogeneity beneath French Polynesia. *Nature* **307**, 536–538.

Wang X.-J., Chen L.-H., Hofmann A. W., Hanyu T., Kawabata H., Zhong Y., Xie L.-W., Shi J.-H., Miyazaki T., Hirahara Y., Takahashi T., Senda R., Chang Q., Vaglarov B. S. and Kimura J.-I. (2018) Recycled ancient ghost carbonate in the Pitcairn mantle plume. *Proc. Natl. Acad. Sci. USA* **115**, 8682–8687.

Weaver B. L. (1991) The origin of ocean island basalt end-member compositions: trace element and isotopic constraints. *Earth Planet. Sci. Lett.* **104**, 381–397.

- Weiss Y., Class C., Goldstein S. L. and Hanyu T. (2016) Key new pieces of the HIMU puzzle from olivines and diamond inclusions. *Nature* **537**, 666–670.
- White W. M. (1985) Sources of oceanic basalts: Radiogenic isotopic evidence. *Geology* **13**, 115–118.
- White W. M. and Hofmann A. W. (1982) Sr and Nd isotope geochemistry of oceanic basalts and mantle evolution. *Nature* **296**, 821–825.
- White W. M. and Duncan R. A. (1996) Geochemistry and geochronology of the Society Islands: New evidence for deep mantle recycling. In *Earth Processes: Reading the Isotopic Code* (eds. A. Basu and S. R. Hart). AGU - Geophysical Monograph Series, Washington D.C. pp. 183–206.
- White W. M., Albarède F. and Télouk P. (2000) High-precision analysis of Pb isotope ratios by multi-collector ICP-MS. *Chem. Geol.* **167**, 257–270.
- Willbold M. and Stracke A. (2010) Formation of enriched mantle components by recycling of upper and lower continental crust. *Chem. Geol.* **276**, 188–197.
- Woodhead J. D. (1996) Extreme HIMU in an oceanic setting: the geochemistry of Mangaia Island (Polynesia), and temporal evolution of the Cook—Austral hotspot. *J. Volcanol. Geotherm. Res.* **72**, 1–19.
- Woodhead J. D. and Devey C. W. (1993) Geochemistry of the Pitcairn seamounts, I: source character and temporal trends. *Earth Planet. Sci. Lett.* **116**, 81–99.
- Woodhead J. D. and McCulloch M. T. (1989) Ancient seafloor signals in Pitcairn Island lavas and evidence for large amplitude, small length-scale mantle heterogeneities. *Earth Planet. Sci. Lett.* **94**, 257–273.
- Zindler A. and Hart S. (1986) Chemical Geodynamics. *Annu. Rev. Earth Planet. Sci.* **14**, 493–571.

**Figure caption**

**Figure 1:** Maps of Pitcairn-Gambier (a) and Society (b) chains, showing the islands investigated in this study. Timing of known volcanic activity is given in My (see Section 2 for references). Along the Pitcairn-Gambier chain, the *Muru* and *Pitis* groups are discriminated from incompatible trace-element and isotope ratios, as explained later in the text (section 5.1.1). Inset: Polynesian island chains, with hotspot location (stars). Figure made with GeoMapApp ([www.geomapapp.org](http://www.geomapapp.org); Ryan et al., 2009).

**Figure 2:** Filtering method for basaltic compositions (shaded area) from all data compiled in this study (see section 4.1 and Fig. S3). The symbol size is used to indicate the distinction between fresh basaltic lavas (large symbols) and other samples (small symbols), while filled/open symbols allow the distinction between new and literature data. Isl.: island, Smt.: seamounts.

**Figure 3:** Incompatible trace-element patterns for representative basalts from Pitcairn-Gambier (a) and Society (b) chains. Abundances are normalized to primitive mantle values of McDonough and Sun (1995). Patterns of the whole sample suite are shown in Figures S4 (Pitcairn-Gambier chain) and S5 (Society chain). Isl.: island, Smt.: seamounts.

**Figure 4:** Plots of (a)  $^{143}\text{Nd}/^{144}\text{Nd}$  versus  $^{87}\text{Sr}/^{86}\text{Sr}$ , (b)  $^{176}\text{Hf}/^{177}\text{Hf}$  versus  $^{143}\text{Nd}/^{144}\text{Nd}$  (mantle array reference line from Chauvel et al., 2008 and Vervoort et al., 2011), (c)  $^{207}\text{Pb}/^{204}\text{Pb}$  versus  $^{206}\text{Pb}/^{204}\text{Pb}$ , and (d)  $^{208}\text{Pb}/^{204}\text{Pb}$  versus  $^{206}\text{Pb}/^{204}\text{Pb}$  for Pitcairn-Gambier and Society basalts, along with fresh basalts of five island chains representative of mantle end-members: St Helena chain and Mangaia, Tubuai and old-Rurutu lavas (Cook-Austral)

represent HIMU basalts; Canary islands, the HIMU-like composition; Walvis ridge, EMI; and Samoa, EM2 (literature data from the GEOROC database).

**Figure 5:**  $Nb_N/Nb^*$ , Ce/Pb and Ba/La as indicators of source composition. (a) and (b) Variations of  $Nb_N/Nb^*$ , Ce/Pb and Ba/La in Pitcairn-Gambier and Society lavas. The three basalt groups (shaded areas) are discussed in the text. (c) and (d) Results of trace-element mixing and batch-melting models. Curves show how  $Nb_N/Nb^*$ , Ce/Pb and Ba/La vary in melts from different sources and with melting degree between 1 and 10% (tick marks each 1% of melting). Source compositions and melting parameters are given in Table S7. The shaded fields show the composition of melts produced by mixing the recycled materials with depleted ambient mantle. The sub-vertical dashed lines highlight the effect of adding 10% of crustal material to the ambient mantle. The HIMU field in panel d (dashed transparent field) corresponds to ratios reported in fresh basalts from St Helena, Mangaia, Tubuai and old-Rurutu lavas (data from the GEOROC database).

**Figure 6:** Plots of  $^{87}Sr/^{86}Sr$  (a),  $^{143}Nd/^{144}Nd$  (b),  $^{176}Hf/^{177}Hf$  (c) and  $^{208}Pb^*/^{206}Pb^*$  (d) versus  $Nb_N/Nb^*$  in Pitcairn-Gambier and Society basalts and in representative OIB.

**Figure 7:** Results of modeling of the isotopic compositions of recycled materials with depending on compositions, ages and subduction fluxes. (a) and (b) Evolution of the Nd-Hf-Pb isotopic compositions with age for different crustal materials and with different sets of values for element mobilities during subduction processes. The oceanic crust forms from the depleted mantle (DMM; Stracke et al., 2003) and then evolves with parent-daughter ratios as measured in N-MORB (normal MORB), E-MORB (enriched MORB) and D-MORB (depleted MORB); all concentrations are from Gale et al. (2013). The effect of N-MORB

dehydration is shown for two sets of values for the element mobility (Stracke et al., 2003 adapted from Kogiso et al., 1997; and Porter and White, 2009). Effects of dehydration and melting on pelagic (Plank and Langmuir, 1998) and terrigenous (Plank, 2014) sediments are calculated using the mobility values of Johnson and Plank (1999). Also shown is the PLUME mantle end-member identified at Hawaii and Galàpagos (Nobre Silva et al., 2013; Harpp and Weis, 2020) and discussed in Section 5.3.2. (c) and (d) Nd-Hf-Pb isotopic composition of the recycled oceanic crust for two contrasted cases of present-day DMM composition (Stracke et al., 2003; Delavault et al., 2015). The isotopic composition of the recycled crust is shifted toward low  $^{143}\text{Nd}/^{144}\text{Nd}$  and  $^{176}\text{Hf}/^{177}\text{Hf}$  but high  $^{206}\text{Pb}/^{204}\text{Pb}$  when using the more depleted DMM of Stracke et al. (2003). Details and parameters for calculation are given in Table S9.

**Figure 8:** Modeling of the potential source of *Muru* basalts. (a)  $\text{TiO}_2$  versus  $^{176}\text{Hf}/^{177}\text{Hf}$  diagram for *Muru* basalts showing the progressive dilution of eclogite at the expense of peridotite-derived melts. (b) Comparison of  $^{176}\text{Hf}/^{177}\text{Hf}$  and  $^{143}\text{Nd}/^{144}\text{Nd}$  in *Muru* basalts with the isotopic composition of mantle sources consisting in a mixture of depleted peridotite and eclogite: 1.5 Gy basaltic crust with 0 to 3 % of modern-like continental sediments as proposed by Delavault et al. (2015) for Gambier basalts. The proportions of eclogite-derived melts are higher than the proportion of eclogite in the source region (5%) proposed by Delavault et al. (2015) by combining olivine and bulk-rock trace elements. (c) Comparison of  $^{176}\text{Hf}/^{177}\text{Hf}$  and Ce/Pb ratios in *Muru* basalts with the composition of melts produced by melting at variable degrees (1 to 10%, thin arrows) enriched material consisting in recycled oceanic crust [OC] of different age, without sediments (filled diamonds) or with 3% sediments (open diamonds). The orange field shows the composition of melts formed by melting a source region made of a mixture of 1.5 Gy-old oceanic crust and DMM (the melting modes are for eclogite for 15% and more of oceanic crust in the mixture, and for peridotite

when less; Table S7). The evolution from Mururoa to Gambier compositions (thick blue arrow) is well explained by the dilution of eclogite with increasing melting degree, but our model suggests low degree melting for the Gambier basalts with high  $^{176}\text{Hf}/^{177}\text{Hf}$  and Ce/Pb ratios, while their low alkalinity and La/Sm<sub>N</sub> ratio call for high melting degree (see Fig. S8). The Lu/Hf ratio of the recycled oceanic crust is considered equal to that of MORB as the mobility of Lu and Hf during subduction is very low (Table S9). DMM (Stracke et al., 2003) is chosen as representative of the ambient material in the plume but we show in panel (d) that it cannot be the case. Unfortunately, the absence of trace-element data for mantle components such as FOZO, PLUME, C or PREMA prevented us from calculating mixtures in panel (c) using such end-members. (d) Mixing curves between oceanic crust and ambient mantle with DMM or PLUME composition in  $^{207}\text{Pb}/^{204}\text{Pb}$  vs  $^{206}\text{Pb}/^{204}\text{Pb}$  space. Tick marks show 15%, 35%, 50% and 75% of eclogite.  $\mu$  is estimated from oceanic crust composition and subduction fluxes given in Table S9.

**Figure 9:** Modeling of the sources of Society and *Pitis* basalts.  $^{176}\text{Hf}/^{177}\text{Hf}$  versus  $^{143}\text{Nd}/^{144}\text{Nd}$  in (a) and versus  $\text{Nb}_\text{N}/\text{Nb}^*$  in (b) showing the position of Society and *Pitis* basalts relative to various potential continental materials involved in their source. In (a), the Nd-Hf evolution with age of oceanic crust, pelagic and terrigenous sediments, and cherts (bold lines) are also shown for comparison. Dashed lines are mixing curves between oceanic crust (age of 1.5 Gy or 2.5 Gy) and terrigenous sediments, pelagic sediments, or Archean cherts. Cordier et al. (2016) suggested an age of 0.5 Gy for the Society enriched material but such young age fails to explain the lowest  $^{176}\text{Hf}/^{177}\text{Hf}$  of Society lavas, given the model parameters presently used. In (b), the colored dotted lines show the composition of the recycled material depending on the proportion of oceanic crust to terrigenous sediments and the black dotted lines show mixing arrays between recycled material (with 3 and 20% sediments) and DMM. In (b), we

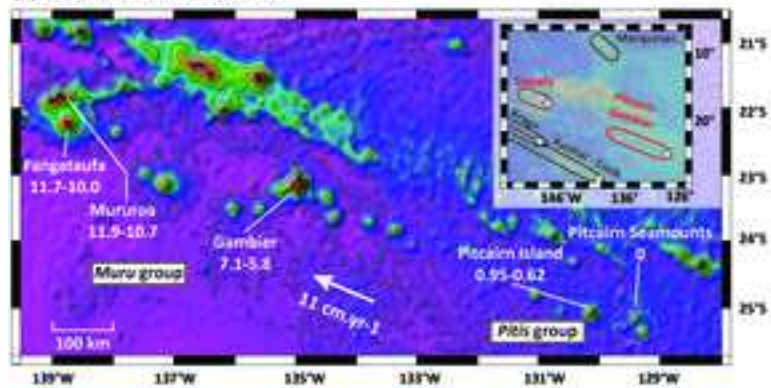
show with the blue line the *Pitis* array. We also show the potential location of the *Pitis* ambient mantle, assuming it has Hf isotope ratio as PLUME/FOZO (Harpp and Weis, 2020) and  $Nb_N/Nb^*$  ratio as Gambier basalts. The mixing array between recycled materials and PLUME/FOZO cannot be calculated because of the lack of trace-element concentration for the PLUME end-member. For all mixing curves, tick marks are every 10% of mixing. See Tables S7 and S9 for model parameters.  $Nb_N/Nb^*$  in cherts is assumed similar as in other continent-derived sediments.

**Figure 10:** Sketch of isotopic changes through time and potential spatial distribution of isotopic heterogeneities in the Polynesian dome. Panels (a) and (b) show the isotopic variations through time along the Society and Pitcairn-Gambier chains. Lavas of each island are assigned the average age of the shield stage (Fig. 1). The isotopic variations are tracked using  $^{143}Nd/^{144}Nd$  for the Society chain because most literature data do not include Hf isotopes. The youngest volcanoes ( $< 1$  My, Moua Pihaa, Teahitia and Mehetia) show a small range compared to other islands of the chain, probably because these volcanoes are still growing. Panel (c) shows a simplified sketch for the possible geometry of heterogeneities in the Polynesian dome. The shape and structure of the dome are drawn from the results of numerical approach of the rising of thermochemical plume (Puckett et al., 2018), while the shallow bending of the Pitcairn-Gambier stem follows the conclusions of French and Romanowicz (2015). We assume that the Polynesian dome anchors at the core/mantle boundary (CMB) and samples the lower Pacific mantle (PLUME/FOZO mantle; dark yellow) together with recycled components with distinct origin and age (bluish shades are for oceanic crust and HIMU/HIMU-like sources; orange, green and purple correspond to continental materials). This large dome entrains some depleted mantle (light yellow shade) when rising (Puckett et al., 2018). It is proposed that the ambient mantle in the Marquesas, Cook-Austral

and Arago plumes is less depleted than DMM (Lassiter et al., 2003; Chauvel et al., 2012; Buff et al., 2021) and we thus assume that it could be similar to the PLUME/FOZO component also identified at Pitcairn-Gambier. See text for discussion of the distribution of the recycled components in each plume and their geometry in the plume stems.

Journal Pre-proofs

(a) PITCAIRN-GAMBIER CHAIN



(b) SOCIETY ISLANDS

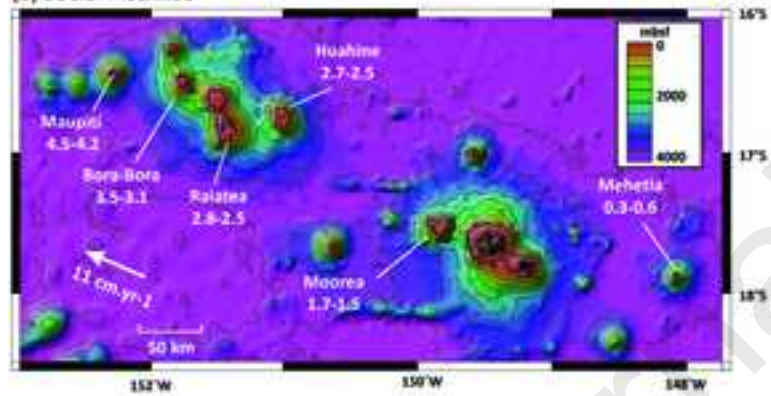


Figure 1

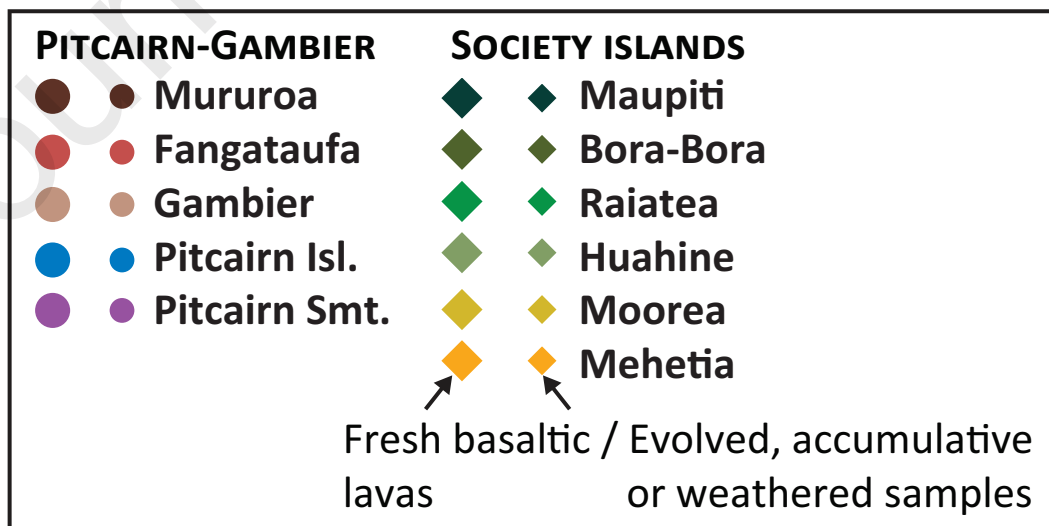
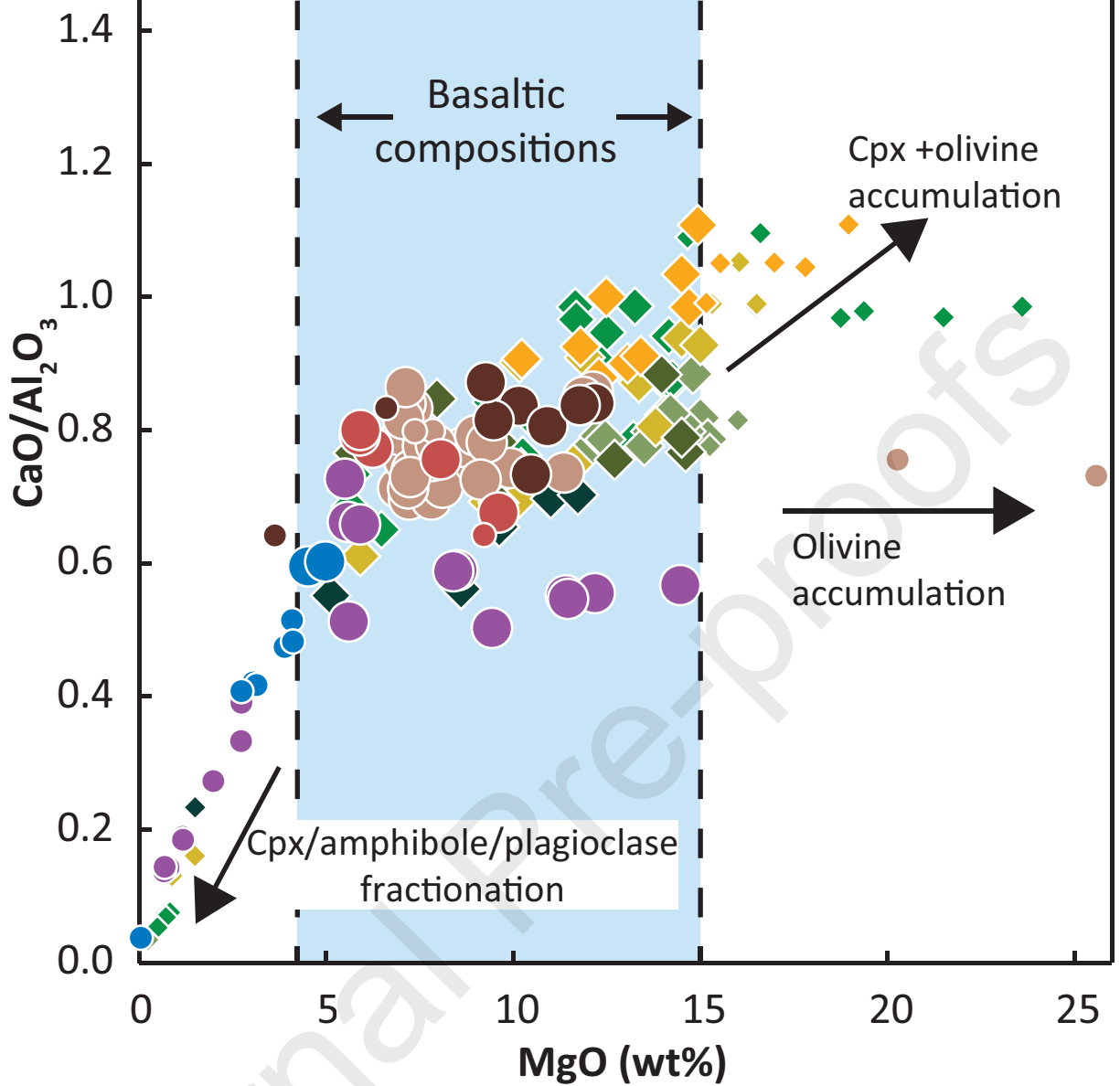


Figure 2

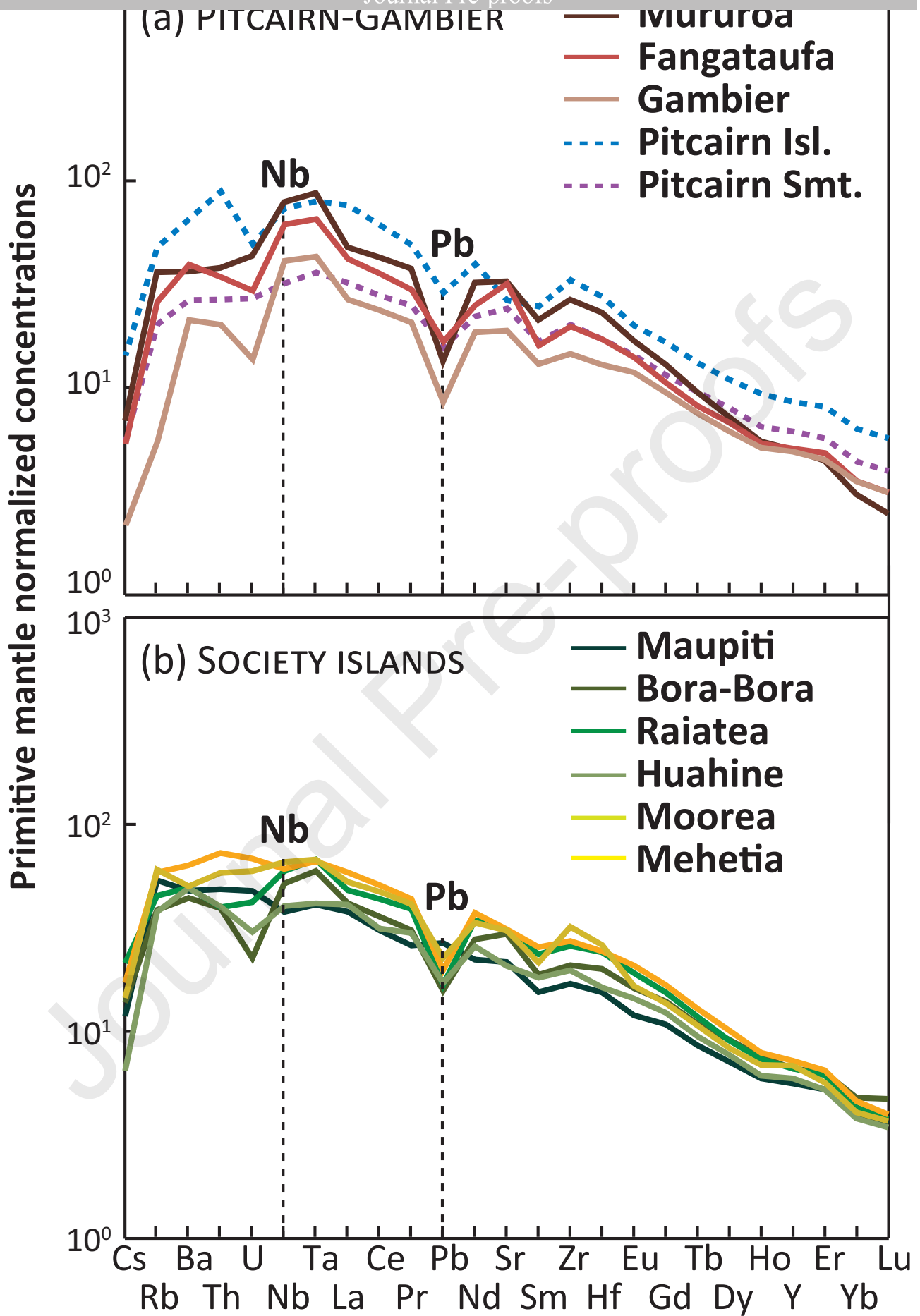


Figure 3

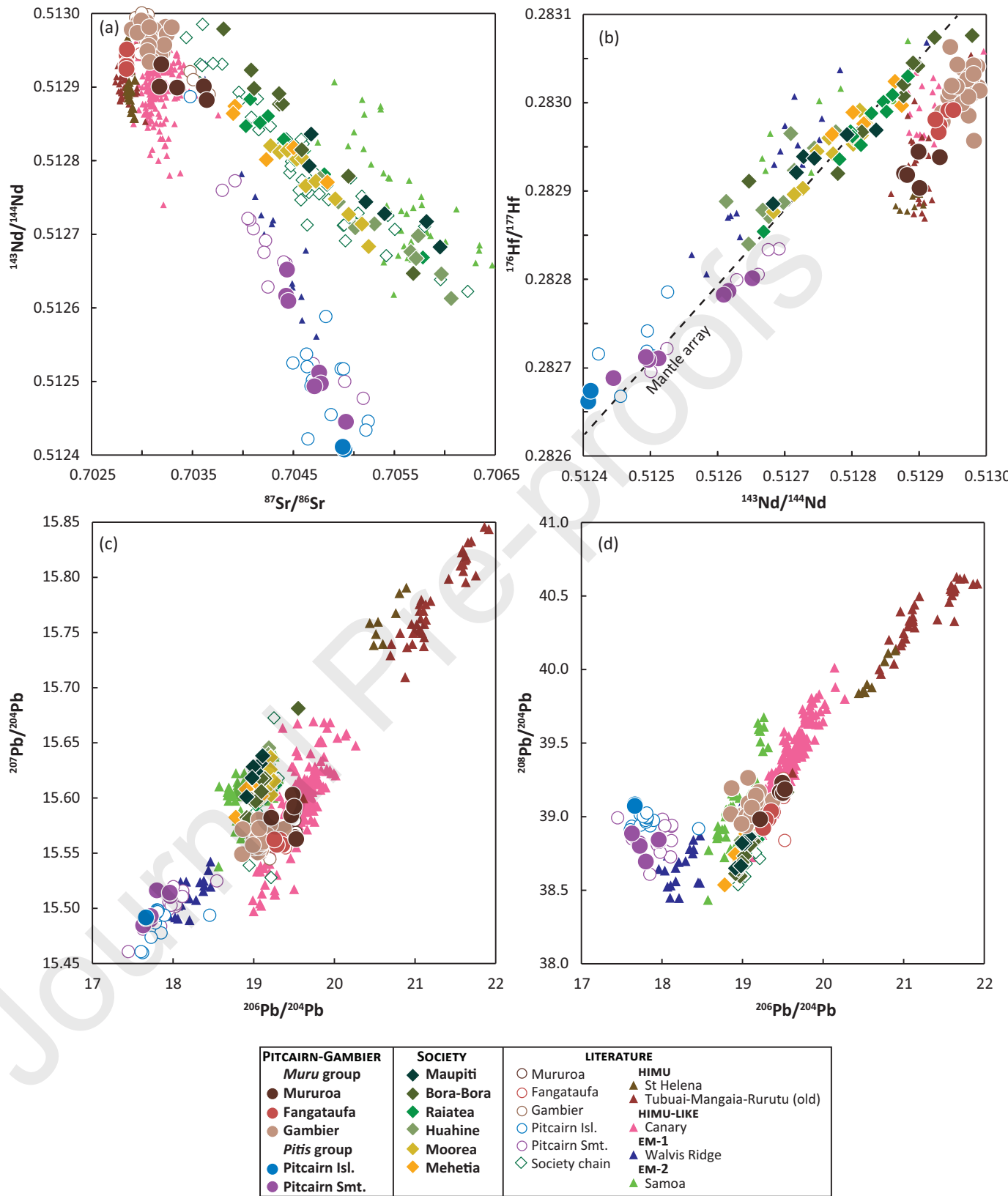
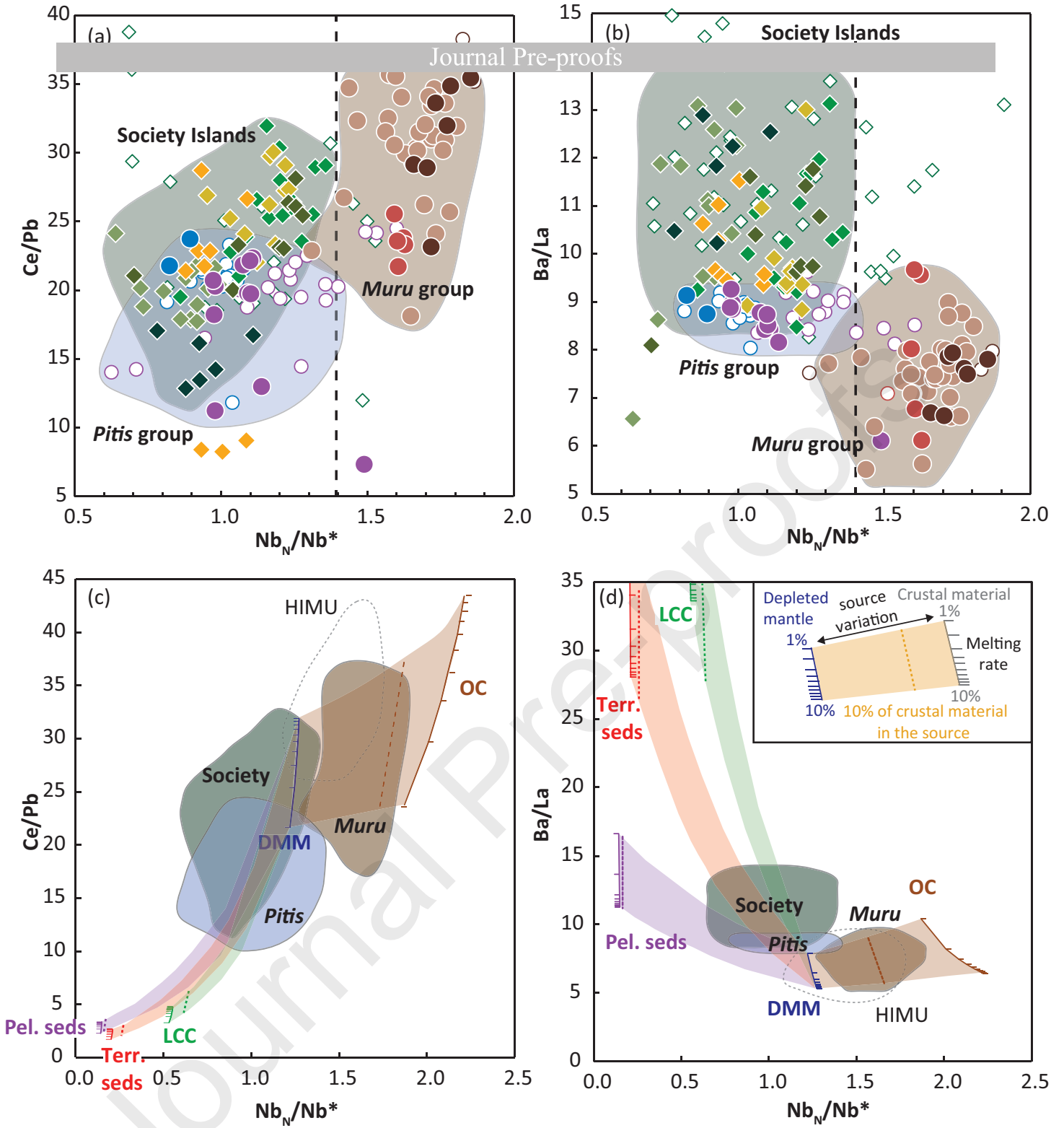


Figure 4



PITCAIRN-GAMBIER	SOCIETY	LITERATURE
<i>Muru group</i>	◆ Maupiti	○ Mururoa
● Mururoa	◆ Bora-Bora	○ Fangataufa
● Fangataufa	◆ Raiatea	○ Gambier
● Gambier	◆ Huahine	○ Pitcairn Isl.
<i>Pitis group</i>	◆ Moorea	○ Pitcairn Smt.
● Pitcairn Isl.	◆ Mehetia	◇ Society chain
● Pitcairn Smt.		

Figure 5

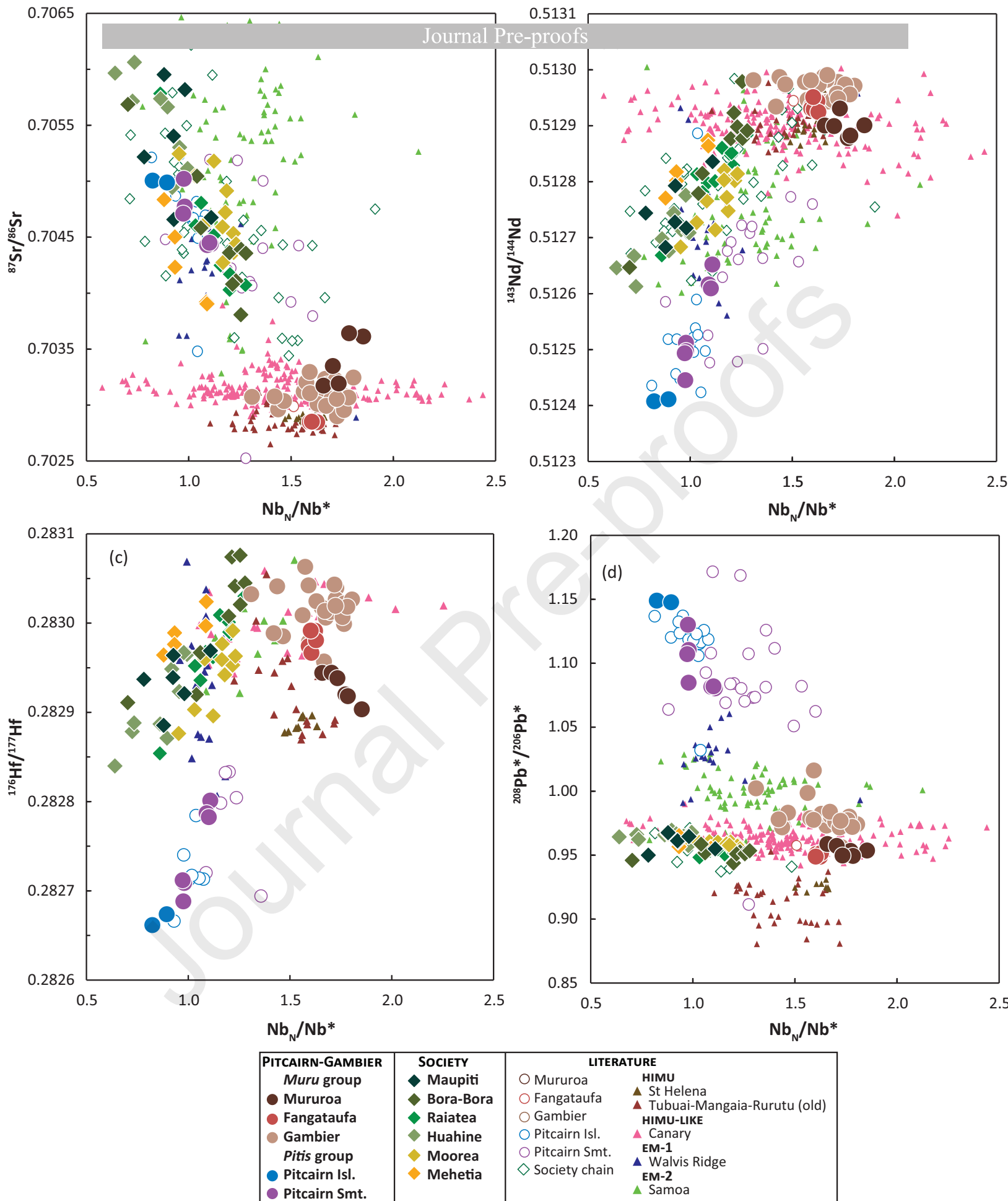


Figure 6

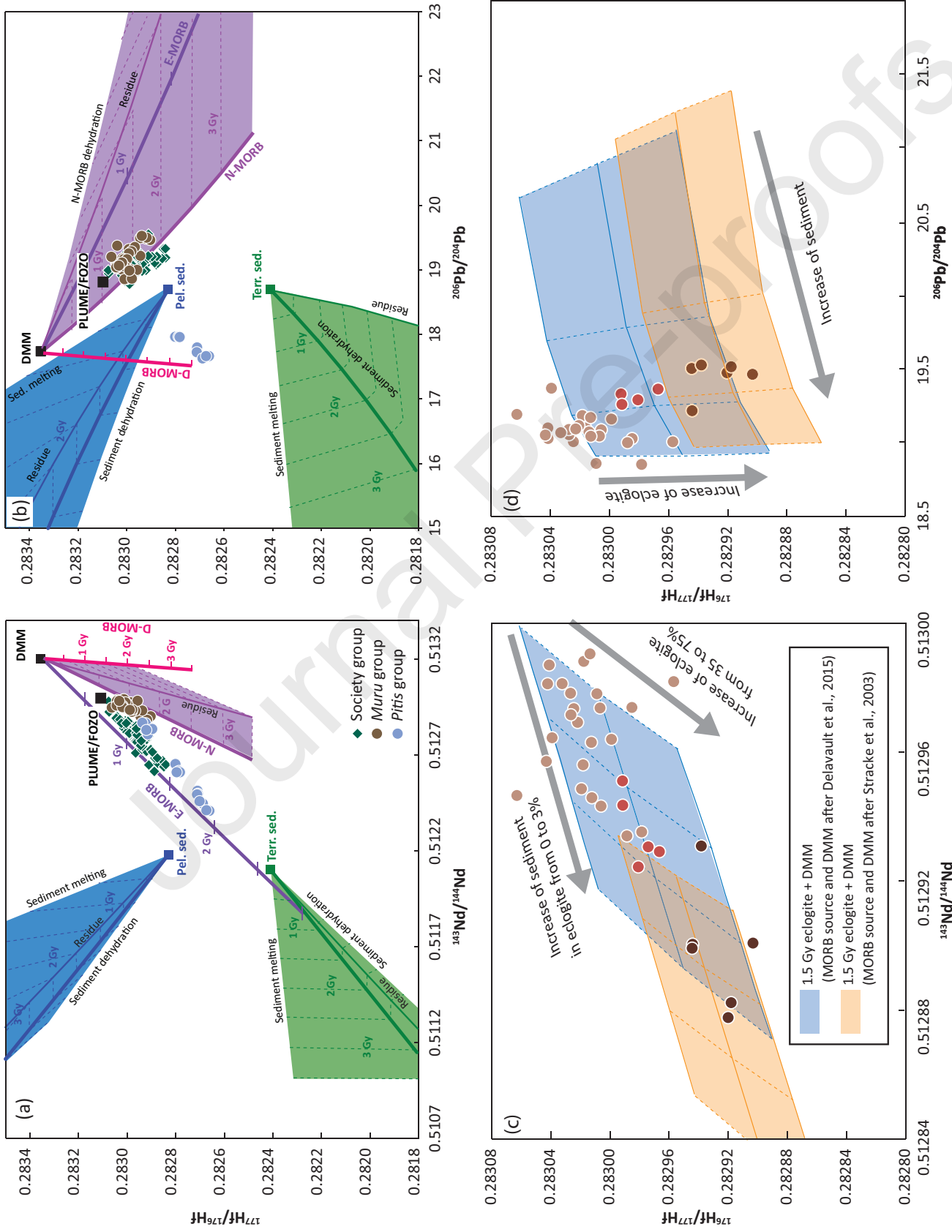


Figure 7

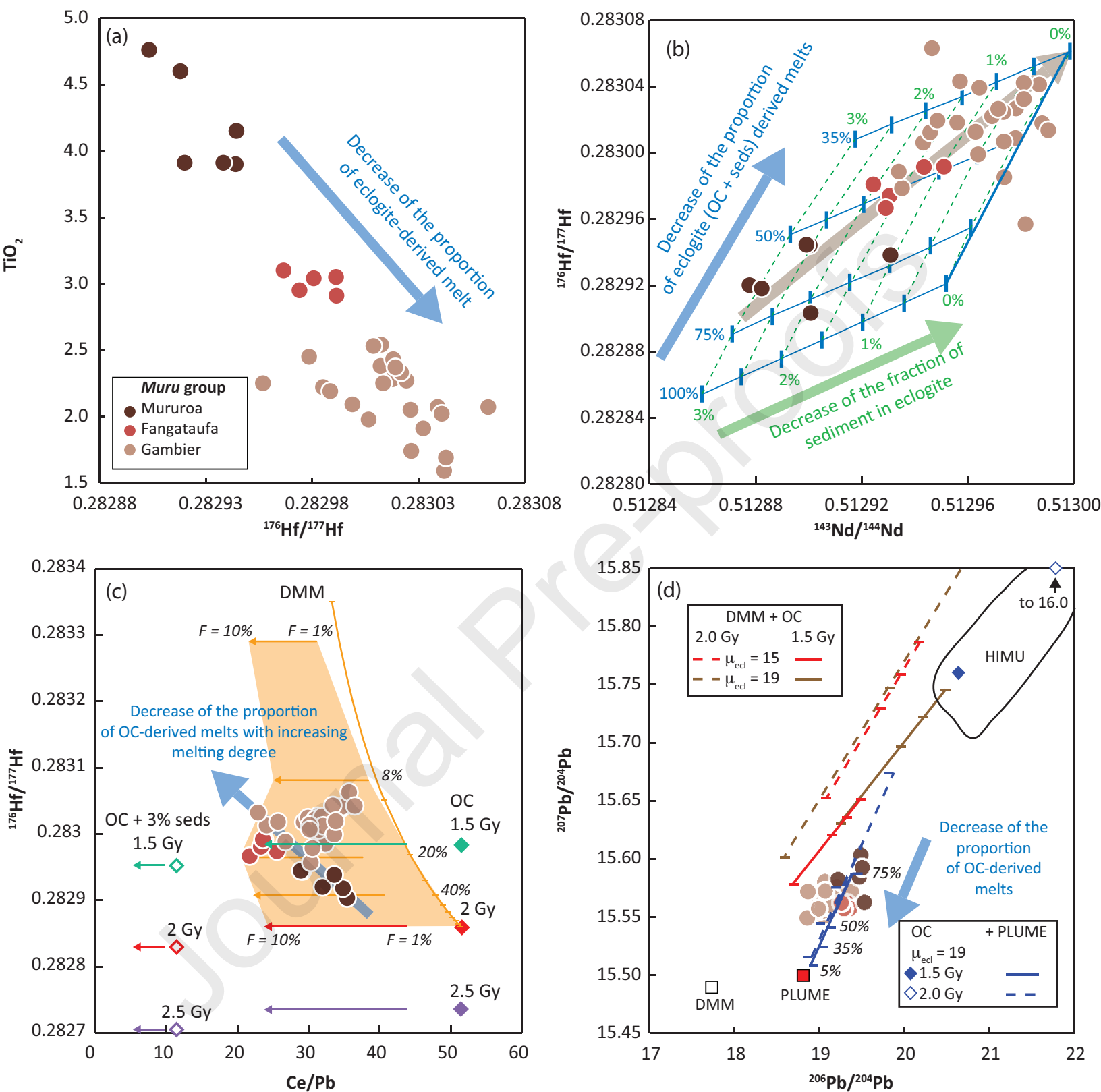


Figure 8

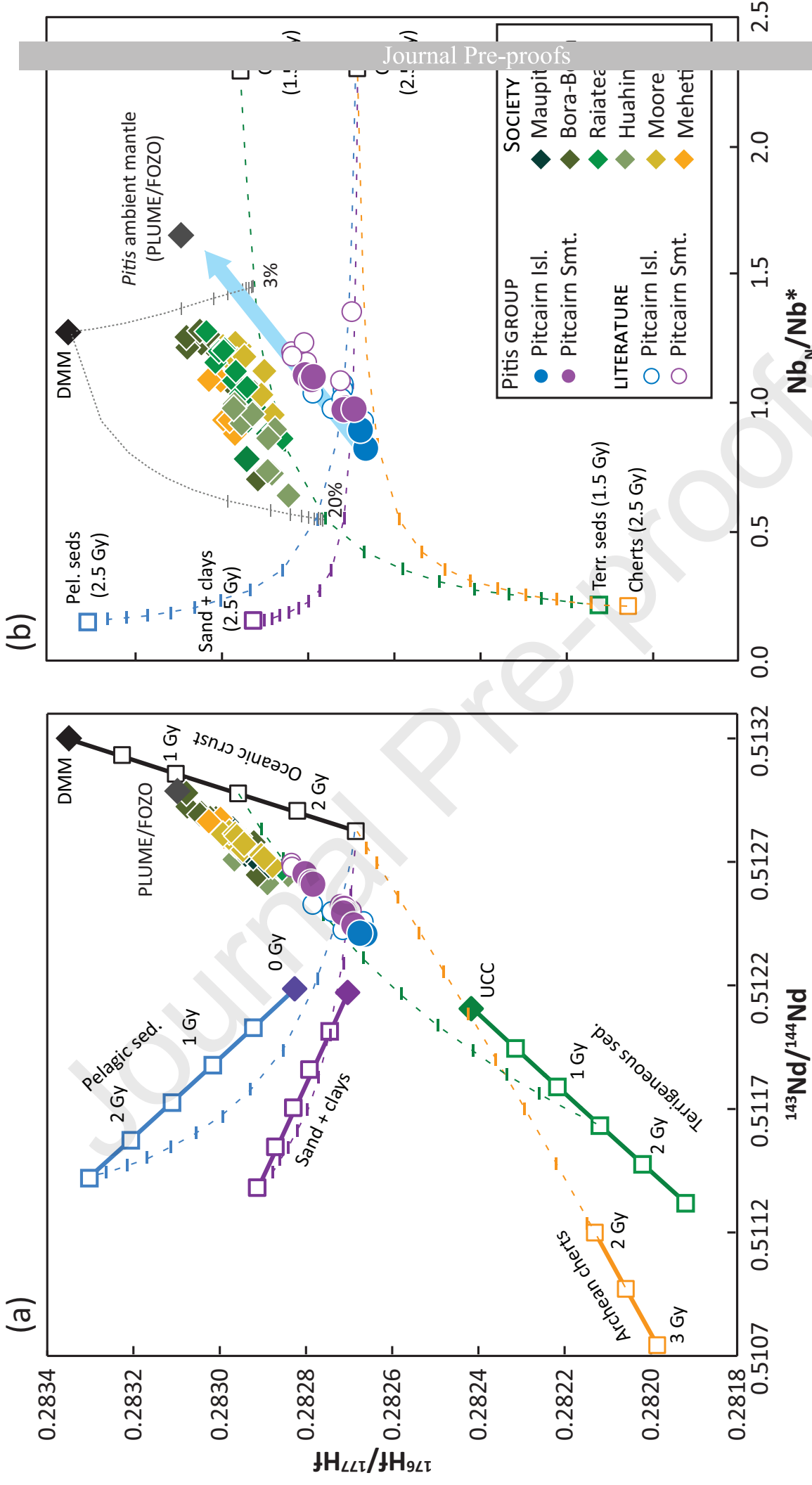


Figure 9

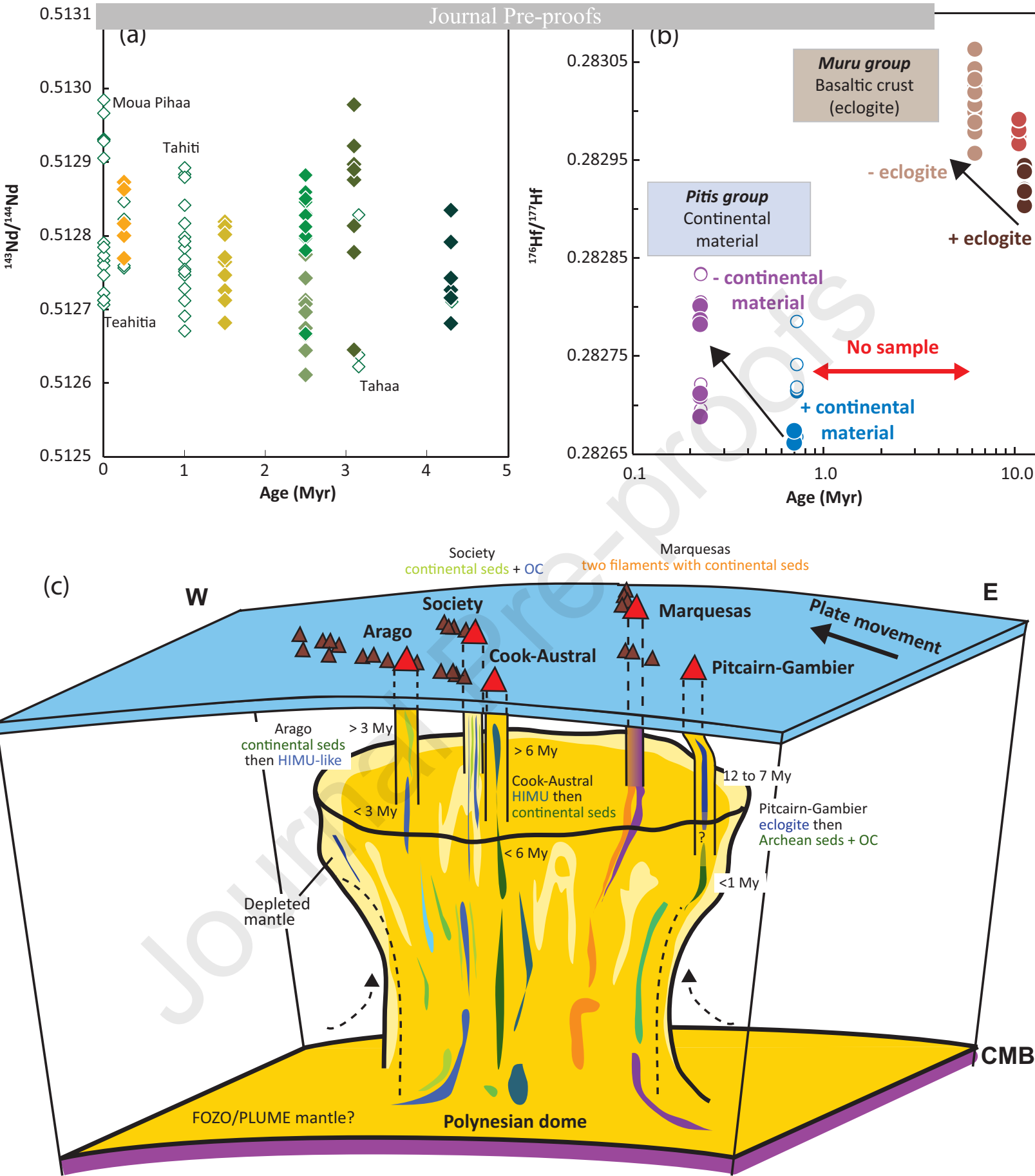


Figure 10

**Declaration of interests**

X The authors declare that they have no known competing financial interests or personal relationships that could have appeared to influence the work reported in this paper.

The authors declare the following financial interests/personal relationships which may be considered as potential competing interests: